Frequency-Packed Faster-Than-Nyquist Signaling via Symbol-Level Precoding for Multiuser MISO Redundant Transmissions

Wallace Alves Martins, *Senior Member, IEEE*, Symeon Chatzinotas, *Senior Member, IEEE*, and Björn Ottersten, *Fellow, IEEE*

***Abstract*— This work addresses the issue of interference generated by co-channel users in downlink multi-antenna multicarrier systems with frequency-packed *faster-than-Nyquist* (FTN) signaling. The resulting interference stems from an aggressive strategy for enhancing the throughput via frequency reuse across different users and the squeezing of signals in the time-frequency plane beyond the Nyquist limit. The spectral efficiency is proved to be increasing with the frequency packing and FTN acceleration factors. The lower bound for the FTN sampling period that guarantees information losslesness is derived as a function of the transmitting-filter roll-off factor, the frequency-packing factor, and the number of subcarriers. Space-time-frequency *symbol-level precoders* (SLPs) that trade off constructive and destructive *interblock interference* (IBI) at the single-antenna user terminals are proposed. Redundant elements are added as guard interval to cope with vestigial destructive IBI effects. The proposals can handle channels with delay spread longer than the multicarrier-symbol duration. The receiver architecture is simple, for it does not require digital multicarrier demodulation. Simulations indicate that the proposed SLP outperforms zero-forcing precoding and achieves a target balance between spectral and energy efficiencies by controlling the amount of added redundancy from zero (full IBI) to half (destructive IBI-free) the group delay of the equivalent channel.**

***Index Terms*— Symbol-level precoding (SLP), multiuser interference (MUI), intercarrier interference (ICI), intersymbol interference (ISI), interblock interference (IBI), faster than Nyquist (FTN), frequency packing, multiple-input single-output (MISO) multicarrier (MC) systems, frequency-selective channels.**

I. Introduction

THE fundamentally limited physical resources of wireless communication systems are the wireless spectrum and transmit power. The exact resource which plays the main role in a specific system design depends largely on the application goals and constraints. In the context of *multiuser* (MU) *multiple-input single-output* (MISO) downlink transmissions, targeting higher data rates is the most common trend, which requires an efficient usage of the available wireless spectrum. From a physical-layer viewpoint, the aggressive frequency reuse across different users as well as the packing of the transmitted signals in the time-frequency plane [1], [2] are amongst the most promising forms of increasing spectral efficiency.

When a multi-antenna base station serves several user terminals, the capacity gains stemming from full frequency-reuse downlink transmissions are greatly affected by the underlying *multiuser interference* (MUI). *Symbol-level precoding* (SLP) [3], [4] encompasses a set of techniques that can benefit from the otherwise harmful MUI effects by shaping the transmitted waveforms so as to induce constructive interference at the user terminals [5]–[8]. SLP is a non-linear technique that employs *channel-state information* (CSI) along with users' data to form the precoder. Several SLP schemes exploiting different properties of the communication environment have been proposed [9]–[12]; the reader is referred to [13] and [14] for further details on SLP.

Besides aggressive frequency reuse, *faster-than-Nyquist* (FTN) signaling [15] has recently been considered as a viable alternative for enhancing spectral efficiency by accelerating the transmission of symbols beyond the Nyquist limit [16]–[18]. Although most FTN schemes focus on compensating the introduced *intersymbol interference* (ISI) at the receiver end [2], some recent works tackle the ISI using precoding techniques [19]–[23] at the transmitter side, which is the focus of our work. When *multicarrier* (MC) systems are employed, one can squeeze the signals in both time and frequency domains [1] via frequency-packed FTN signaling, and very few works have exploited this fact along with precoding designs [21], [22]. The authors in [21] have proposed an MU-MISO spectrally efficient frequency division multiplexing (SEFDM) scheme comprising a two-stage waveform and space precoding architecture for frequency-packed MC systems. The waveform precoding pre-equalizes the self-created *intercarrier interference* (ICI) within the waveform due to frequency-packing, whereas the space precoding pre-cancels the spatial MUI. The authors in [22] have proposed a linear precoding scheme to be used in point-to-point scenarios, but

Manuscript received 14 July 2021; revised 3 November 2021 and 10 February 2022; accepted 14 April 2022. Date of publication 25 April 2022; date of current version 11 October 2022. This work was supported in part by the Luxembourg National Research Fund (FNR)—RISOTTI: Reconfigurable intelligent surfaces for smart cities, under Grant FNR/C20/IS/14773976/RISOTTI and in part by the CI-PHY: Exploiting interference for physical layer security in 5G networks, under Grant FNR/INTER/FNR-RCUK/17/11607830. The associate editor coordinating the review of this article and approving it for publication was T. Tsiftsis. *(Corresponding author: Wallace Alves Martins.)*

The authors are with the Interdisciplinary Centre for Security Reliability and Trust (SnT), University of Luxembourg, 1855 Luxembourg, Luxembourg (e-mail: wallace.alvesmartins@uni.lu; symeon.chatzinotas@uni.lu; bjorn.ottersten@uni.lu).

Color versions of one or more figures in this article are available at https://doi.org/10.1109/TWC.2022.3168188.

Digital Object Identifier 10.1109/TWC.2022.3168188

This work is licensed under a Creative Commons Attribution 4.0 License. For more information, see https://creativecommons.org/licenses/by/4.0/

its generalization to MU communications is still an open problem.

It is worth noting that MC-modulated signals are commonly used in broadband communications to overcome the challenges imposed by frequency-selective channels. MC systems usually employ variations of the well-known *orthogonal frequency-division multiplexing* (OFDM) [24]. Although most OFDM-based schemes focus on compensating ISI at the receiver end, it is possible to adapt well-known precoders, such as *maximum ratio transmitter* (MRT) [25] and *zero-forcing* (ZF) [26], to the multicarrier case, considering the equivalent model of parallel flat-fading channels obtained from a convenient introduction of guard intervals. In this case, the guard-interval length is larger than the equivalent channel order.

Conventional precoders usually handle MUI only in the spatial domain. This also applies to OFDM systems thanks to their equivalent parallel flat-fading model. When such a model is not suitable, the users' data, which are split into subcarriers (frequency domain) and are transmitted using an antenna array (spatial domain), may experience both spatial interference and ICI, besides ISI stemming from FTN accelerated transmissions. Space-time-frequency precoding is, therefore, called for. In fact, the design of space-time-frequency SLP techniques that induce constructive interference at the receivers is an open problem as of yet. A key aspect in such an open problem is to address how these schemes can cope with the *interblock interference* (IBI) inherent in frequency-selective channels.

In this work, we address this open problem by proposing a new MU-MISO system model that tackles the frequency-selectivity-related IBI, ISI, and ICI effects using space-time-frequency SLPs. We adapt to the non-linear setup some ideas from reduced-redundancy linear transceivers [27]–[33], and design redundant space-time-frequency SLPs that minimize the total transmit power while allowing for the trade-off between constructive and destructive IBI effects. Redundant elements are added as guard interval to cope with vestigial destructive IBI effects. In order to reduce the impact on spectral efficiency, the amount of added redundancy may vary from zero (full IBI) to half (destructive IBI-free) the group delay of the equivalent channel model. Thus, in addition to saving bandwidth as compared to conventional OFDM-based systems (since the group delay is usually much smaller than the channel order, and we use at most half the group delay as guard-interval length), the proposed precoders also simplify the receiver architecture by relieving it of performing *discrete Fourier transform* (DFT) computations, as it will be further detailed. We also characterize mathematically the behavior of the spectral efficiency (i.e., the achievable data rate, or maximum throughput, normalized by the bandwidth) showing its monotonicity with respect to the sampling time and frequency-packing factor. We derive the minimum admissable sampling time that allows for information losslessness [23] as a function of the frequency-packing factor, the number of subcarriers, and the roll-off factor of the transmiting/receiving filters. We also provide the relations among important variables, like the minimum guard-interval length that enables destructive IBI-free transmissions as a function of the group delay of the effective channel, as well as the exact number of backward and forward IBI-related blocks affecting the signal reconstruction at the receiver end.

The paper is organized as follows. An MU-MISO system model of a multicarrier linear ZF precoder is described in Section II. A set of new results along with detailed discussions regarding frequency-packed FTN signaling are provided in Section III. A new MU-MISO multicarrier system is proposed in Section IV along with the non-linear space-time-frequency SLP. The performance of the proposed precoders is assessed through numerical experiments in Section V. The concluding remarks are in Section VI.

Notation: Scalars are denoted by italic letters, whereas vectors and matrices are denoted by boldface letters (lowercase for vectors and uppercase for matrices). Calligraphic letters denote sets. Discrete-time signals are expressed with brackets and continuous-time signals with parentheses; $\delta[n]$ is the Kronecker discrete-time pulse, whereas $\delta(t)$ is the Dirac continuous-time impulse. The Fourier transform of $f(t)$ is denoted as $F(\mathrm{j}\omega)$, wherein $\mathrm{j}^2 = -1$. The symbols $\triangleq$ and $*$ denote definition assignment and linear convolution, respectively, whereas $\otimes$ and $\odot$ denote Kronecker and Hadamard products, respectively. The notations $(\cdot)^{\intercal}$ and $(\cdot)^{\mathrm{H}}$ stand for transpose and Hermitian transpose operations on $(\cdot)$, respectively. The real and imaginary parts of a complex number $z = a + \mathrm{j}b$ are respectively denoted by $\Re\{z\} = a$ and $\Im\{z\} = b$. If $\boldsymbol{x}$ is a vector, then $[\boldsymbol{x}]_n$ denotes its n^{th} entry. Given a real number x, $\lfloor x \rfloor$ and $\lceil x \rceil$ respectively stand for the largest integer smaller than or equal to x and the smallest integer greater than or equal to x.

II. Multicarrier Precoding Preliminaries

A. System Model

Consider the base-band MU-MISO system model of a downlink multicarrier transmission to K single-antenna user terminals via $N \geq K$ antennas illustrated in Fig. 1.

For the precoding design, we will assume perfect CSI knowledge at the transmitter side. The system works in a block-based manner, so that the data stream to be delivered to the k^{th} user is divided into non-overlapping blocks with M symbols from a complex-valued constellation $\mathcal{C}$. Let $s_k[m] \in \mathcal{C}$, with $m \in \mathscr{M} \triangleq \{0, 1, \ldots, M-1\}$, denote the constellation symbols of one block to be transmitted to the k^{th} user, and $\boldsymbol{s}_k$ denote a vector gathering the M symbols of the block. All vectors $\boldsymbol{s}_k$, with $k \in \mathscr{K} \triangleq \{0, 1, \ldots, K-1\}$, are linearly processed jointly by the zero-forcing precoder to yield the precoded vectors $\boldsymbol{d}_n \in \mathbb{C}^{M\times 1}$, with $n \in \mathscr{N} \triangleq \{0, 1, \ldots, N-1\}$. Each precoded vector $\boldsymbol{d}_n$ passes through a digital multicarrier modulator implemented via an *inverse DFT* (IDFT) operation, followed by a redundancy insertion block, thus generating the vector $\boldsymbol{x}_n \in \mathbb{C}^{P\times 1}$, in which $P \triangleq M + R$, with R denoting the number of redundant elements added as guard interval in the form of *zero padding* (ZP).

The continuous-time signal $\tilde{x}_n(t)$ that feeds the RF chain of the n^{th} antenna element is the output of a *digital-to-analog converter* (DAC) with sampling time T_{s}; thus, by defining the index set $\mathscr{P} \triangleq \{0, 1, \ldots, P-1\}$, one has

$$\tilde{x}_n(t) \triangleq \sum_{p\in\mathscr{P}} x_n[p] \cdot f(t - pT_{\mathrm{s}}) = (x_n * f)(t), \qquad (1)$$

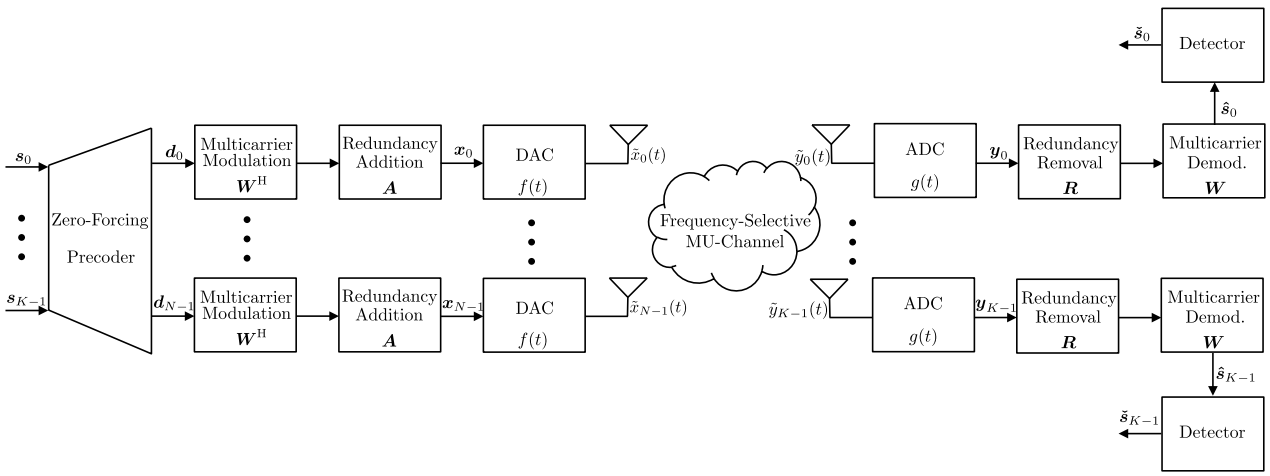

Fig. 1. Multiuser MISO base-band model of a linear zero-forcing precoder.

where $f(t)$ denotes the transmitting pulse (e.g., a *square-root raised cosine*—SRRC) and

$$x_n(t) \triangleq \sum_{p\in\mathscr{P}} x_n[p]\cdot\delta(t-pT_{\rm s}). \tag{2}$$

Let us assume a frequency-selective channel whose coherence time is longer than the duration for transmitting one block of signals, and let $\tilde{h}_{k,n}(t)$ denote the impulse response of the base-band physical link between the $n^{\rm th}$ transmitting antenna and the $k^{\rm th}$ user terminal. The base-band signal received by the $k^{\rm th}$ user is

$$\tilde{y}_k(t) \triangleq \sum_{n\in\mathscr{N}} \left(\tilde{h}_{k,n} * \tilde{x}_n\right)(t) + \tilde{v}_k(t), \tag{3}$$

in which $\tilde{v}_k(t)$ is an additive noise signal.

The signal at the output of the receiving filter $g(t)$ is

$$y_k(t) \triangleq \sum_{n\in\mathscr{N}}\sum_{p\in\mathscr{P}} x_n[p]\cdot h_{k,n}(t-pT_{\rm s}) + v_k(t), \tag{4}$$

in which $v_k(t) \triangleq (g * \tilde{v}_k)(t)$ is the equivalent noise and

$$h_{k,n}(t) \triangleq (\tilde{h}_{k,n} * g * f)(t) \tag{5}$$

is the equivalent base-band channel model. After sampling the signal $y_k(t)$, the resulting samples are collected in the vector $\boldsymbol{y}_k \in \mathbb{C}^{P\times 1}$ and then processed via a redundancy removal step, followed by a multicarrier demodulation implemented via a DFT operation, before the actual symbol detection.

B. Linear ZF Precoder

When dealing with standard linear ZF precoders, it is implicitly assumed that R is sufficiently large so that the redundancy addition at the transmitter and removal at the receiver are able to eliminate IBI as well as to induce a circulant-channel structure for each equivalent link between transmitting antennas and user terminal.

At the receiver side, after the redundancy removal the resulting signal is multiplied by the M-dimensional unitary DFT matrix $\boldsymbol{W}$, which combined with the IDFT in the transmitter, is able to diagonalize the corresponding equivalent channel matrix [24]. Hence, one can write the estimated symbols of the $k^{\rm th}$ user as

$$\hat{\boldsymbol{s}}_k = \sum_{n\in\mathscr{N}} \boldsymbol{\Lambda}_{k,n}\boldsymbol{d}_n + \boldsymbol{z}_k, \tag{6}$$

where $\boldsymbol{\Lambda}_{k,n}$ is an $M\times M$ diagonal matrix containing the frequency response of the equivalent channel between the $n^{\rm th}$ antenna element and the $k^{\rm th}$ user terminal [24], and $\boldsymbol{z}_k$ is the equivalent additive noise.

Thus, one has the following complete model:

$$\underbrace{\begin{bmatrix}\hat{\boldsymbol{s}}_0\\ \vdots\\ \hat{\boldsymbol{s}}_{K-1}\end{bmatrix}}_{\triangleq\hat{\boldsymbol{s}}\in\mathbb{C}^{MK\times 1}} = \underbrace{\begin{bmatrix}\boldsymbol{\Lambda}_{0,0} & \cdots & \boldsymbol{\Lambda}_{0,N-1}\\ \vdots & \vdots & \vdots\\ \boldsymbol{\Lambda}_{K-1,0} & \cdots & \boldsymbol{\Lambda}_{K-1,N-1}\end{bmatrix}}_{\triangleq\boldsymbol{H}\in\mathbb{C}^{MK\times MN}} \underbrace{\begin{bmatrix}\boldsymbol{d}_0\\ \vdots\\ \boldsymbol{d}_{N-1}\end{bmatrix}}_{\triangleq\boldsymbol{d}\in\mathbb{C}^{MN\times 1}} + \underbrace{\begin{bmatrix}\boldsymbol{z}_0\\ \vdots\\ \boldsymbol{z}_{K-1}\end{bmatrix}}_{\triangleq\boldsymbol{z}\in\mathbb{C}^{MK\times 1}} \tag{7}$$

or, simply,

$$\hat{\boldsymbol{s}} = \boldsymbol{H}\boldsymbol{d} + \boldsymbol{z}. \tag{8}$$

The ZF precoded signals are therefore obtained as [26]

$$\boldsymbol{d} = \boldsymbol{H}^{\rm H}\left(\boldsymbol{H}\boldsymbol{H}^{\rm H}\right)^{-1}\boldsymbol{s}, \tag{9}$$

wherein $\boldsymbol{s} \triangleq \left[\,\boldsymbol{s}_0^{\mathsf{T}} \;\cdots\; \boldsymbol{s}_{K-1}^{\mathsf{T}}\,\right]^{\mathsf{T}}$. Note that, due to the structure of $\boldsymbol{H}$, the signals $s_k[m]$ modulating the $m^{\rm th}$ subcarrier are spatially combined for all users $k\in\mathscr{K}$ without exchanging data among subcarriers (spatial-domain precoding). In other words, this multicarrier model is equivalent to M parallel single-carrier precoded transmissions. Indeed, the $m^{\rm th}$ entry of vector $\hat{\boldsymbol{s}}_k$ in (7) can be written as

$$\hat{s}_k[m] = \left(\boldsymbol{\lambda}_k^{(m)}\right)^{\mathsf{T}}\boldsymbol{d}^{(m)} + z_k[m], \quad \forall m\in\mathscr{M}, \tag{10}$$

where $\boldsymbol{\lambda}_k^{(m)} \in \mathbb{C}^{N\times 1}$ collects the $m^{\rm th}$ diagonal entry of all the N matrices $\boldsymbol{\Lambda}_{k,n}$, with $n\in\mathscr{N}$, whereas $\boldsymbol{d}^{(m)} \in \mathbb{C}^{N\times 1}$ collects the $m^{\rm th}$ entry (corresponding to the $m^{\rm th}$ subcarrier) of

all the N precoded vectors $\boldsymbol{d}_n$, with $n \in \mathscr{N}$. Now, considering all the K users, one gets

$$\underbrace{\begin{bmatrix} \hat{s}_0[m] \\ \vdots \\ \hat{s}_{K-1}[m] \end{bmatrix}}_{\triangleq \hat{\boldsymbol{s}}^{(m)} \in \mathbb{C}^{K\times 1}} = \underbrace{\begin{bmatrix} \left(\boldsymbol{\lambda}_0^{(m)}\right)^{\mathsf{T}} \\ \vdots \\ \left(\boldsymbol{\lambda}_{K-1}^{(m)}\right)^{\mathsf{T}} \end{bmatrix}}_{\triangleq \boldsymbol{H}^{(m)} \in \mathbb{C}^{K\times N}} \boldsymbol{d}^{(m)} + \underbrace{\begin{bmatrix} z_0[m] \\ \vdots \\ z_{K-1}[m] \end{bmatrix}}_{\triangleq \boldsymbol{z}^{(m)} \in \mathbb{C}^{K\times 1}}, \forall m \in \mathscr{M}, \tag{11}$$

or, simply,

$$\hat{\boldsymbol{s}}^{(m)} = \boldsymbol{H}^{(m)}\boldsymbol{d}^{(m)} + \boldsymbol{z}^{(m)}, \quad \forall m \in \mathscr{M}. \tag{12}$$

Therefore, the (per-subcarrier) ZF precoded signals can alternatively be written as

$$\boldsymbol{d}^{(m)} = \left(\boldsymbol{H}^{(m)}\right)^{\mathrm{H}} \left[\boldsymbol{H}^{(m)}\left(\boldsymbol{H}^{(m)}\right)^{\mathrm{H}}\right]^{-1} \boldsymbol{s}^{(m)}, \quad \forall m \in \mathscr{M}, \tag{13}$$

wherein $\boldsymbol{s}^{(m)} \triangleq [\, s_0[m] \ \cdots \ s_{K-1}[m]\,]^{\mathsf{T}}$.

C. Remarks

Usually, $(f * g)(t)$ is a T_1-Nyquist filter with roll-off factor $\rho \in (0, 1]$ and period $T_1 > 0$, so that no additional ISI is induced as long as: (i) $T_{\mathrm{s}} = T_1$; (ii) the received signal employs the same sampling time T_{s}; and (iii) there is no time offset. Indeed, $(f * g)(pT_1) \propto \delta[p - \delta_0]$, where δ_0 is a discrete-time delay; this means the transmitting/receiving filters spread the signal in time without inducing interference among the samples spaced apart at multiples of T_1. However, when attempting to increase throughput by increasing the baud-rate making $T_{\mathrm{s}} < T_1$, one may end up with an equivalent channel for which the number of redundant elements R is not sufficient to guarantee complete IBI elimination. In fact, the residual interference might be significant enough to impair the overall system performance in terms of bit-error rate or throughput.

The next section addresses the case in which the transmission of signals are frequency-packed by using fractional Fourier transform and accelerated by using a sampling time $T_{\mathrm{s}} < T_1$.

III. Frequency-Packed Faster-Than-Nyquist Signaling

Let us start by analyzing the spectrum of the transmitted signals for the system model in Section II-A. The Fourier transform of the base-band transmitted signal in (1) is

$$\tilde{X}_n(\mathrm{j}\Omega) = X_n\left(\mathrm{e}^{\mathrm{j}\Omega T_{\mathrm{s}}}\right) F(\mathrm{j}\Omega), \tag{14}$$

where $X_n\left(\mathrm{e}^{\mathrm{j}\omega}\right)$ is the *discrete-time Fourier transform* (DTFT) of the sequence $x_n[m]$, with $m \in \mathscr{M}$. When expressing the corresponding continuous-time Fourier transform, one has that $X_n\left(\mathrm{e}^{\mathrm{j}\Omega T_{\mathrm{s}}}\right)$ is $\frac{2\pi}{T_{\mathrm{s}}}$-periodic, so that one can state that the entire information about the signal is, for instance, within the low-pass band $\left[0, \frac{2\pi}{T_{\mathrm{s}}}\right)$ rad/s. Being more specific, one has

$$X_n\left(\mathrm{e}^{\mathrm{j}\omega}\right) = \textstyle\sum_{m' \in \mathscr{M}} d_n[m'] \mathrm{DTFT}\left\{\frac{1}{\sqrt{M}} \mathrm{e}^{\mathrm{j}\frac{2\pi}{M}mm'}\right\}, \tag{15}$$

and by defining the window $w[m] = \frac{1}{\sqrt{M}}$, for all $m \in \mathscr{M}$, and $w[m] = 0$ otherwise, then one can write

$$\mathrm{DTFT}\left\{w[m]\mathrm{e}^{\mathrm{j}\frac{2\pi}{M}mm'}\right\} = W\left(\mathrm{e}^{\mathrm{j}\left(\omega - \frac{2\pi}{M}m'\right)}\right), \quad \forall m' \in \mathscr{M}, \tag{16}$$

where

$$W\left(\mathrm{e}^{\mathrm{j}\omega}\right) \triangleq \frac{\mathrm{e}^{-\mathrm{j}\omega\left(\frac{M-1}{2}\right)}}{\sqrt{M}} \frac{\sin\left(\frac{\omega M}{2}\right)}{\sin\left(\frac{\omega}{2}\right)}. \tag{17}$$

Although the support of the 2π-periodic function $W\left(\mathrm{e}^{\mathrm{j}\omega}\right)$ spans, for instance, the whole interval $[0, 2\pi)$ rad/sample, let us assume for the sake of discussion that the main lobe of $W\left(\mathrm{e}^{\mathrm{j}\omega}\right)$ essentially defines its bandwidth, which is therefore $\frac{2\pi}{M}$. Thus, the bandwidth of $X_n\left(\mathrm{e}^{\mathrm{j}\omega}\right)$ in terms of normalized frequency in the range $[0, 2\pi)$ rad/sample is

$$\frac{2\pi}{M}(M-1) + \frac{2\pi}{M} = 2\pi, \tag{18}$$

which shows that, no matter the number of subcarriers M, the MC-modulated signal is full-band and, therefore, the continuous-time signal before the pulse shaping, $x_n(t)$, occupies the entire band $\left[0, \frac{2\pi}{T_{\mathrm{s}}}\right)$ rad/s.

A. Frequency-Packed Transmissions

One can attempt to increase the spectrum efficiency of the MC-modulated scheme in Fig. 1 by replacing the IDFT matrix in the transmitter side with the so-called *inverse fractional Fourier transform* (IFrFT) matrix $\boldsymbol{W}_{\beta}^{\mathrm{H}}$ [34]—see the proposed transmitter structure in Fig. 2 on p. 8666. The entry $(m, m') \in \mathscr{M}^2$ of the IFrFT matrix is $\mathrm{e}^{\mathrm{j}\frac{2\pi\beta}{M}mm'}$, wherein $\beta \in (0, 1]$ is a parameter that controls the frequency packing. In addition, considering a post-IFrFT modulation by $w[m]\mathrm{e}^{-\mathrm{j}\pi\beta\left(\frac{M-1}{M}\right)m}$, the entry (m, m) of the diagonal matrix $\boldsymbol{\Sigma}_{\beta}$ in Fig. 2, which shifts the frequency-domain content so that the center frequency is now at 0 rad (instead of π rad),[1] then one has

$$X_n\left(\mathrm{e}^{\mathrm{j}\omega}\right) = \sum_{m' \in \mathscr{M}} d_n[m'] \, \mathrm{DTFT}\left\{w[m]\mathrm{e}^{-\mathrm{j}\pi\beta\left(\frac{M-1}{M}\right)m}\mathrm{e}^{\mathrm{j}\frac{2\pi\beta}{M}mm'}\right\}, \tag{19}$$

where

$$\mathrm{DTFT}\left\{w[m]\mathrm{e}^{-\mathrm{j}\pi\beta\left(\frac{M-1}{M}\right)m}\mathrm{e}^{\mathrm{j}\frac{2\pi\beta}{M}mm'}\right\} = W\left(\mathrm{e}^{\mathrm{j}\left(\omega - \beta\frac{2\pi}{M}(m' - (M-1)/2)\right)}\right), \quad \forall m' \in \mathscr{M}, \tag{20}$$

so that the bandwidth of $X_n\left(\mathrm{e}^{\mathrm{j}\omega}\right)$ in the range $[-\pi, \pi)$ rad/sample is now

$$\beta\frac{2\pi}{M}(M-1) + \frac{2\pi}{M} = 2\pi \cdot \underbrace{\left(\frac{M-1}{M}\beta + \frac{1}{M}\right)}_{\triangleq \xi_M(\beta)} = 2\pi\xi_M(\beta), \tag{21}$$

[1]The modulation by $\mathrm{e}^{-\mathrm{j}\pi\beta\left(\frac{M-1}{M}\right)m}$ is particularly important when accelerating the transmissions via FTN, since the magnitude response of the transmitting filter, $|F(\mathrm{j}\Omega)|$, is symmetric around the origin.

in which $\xi_M(\beta) < 1$ for any $\beta \in (0,1)$ as long as $M > 1$, whereas $\xi_M(1) = 1$ for any $M \geq 1$. Therefore, the continuous-time signal before the pulse shaping, $x_n(t)$, essentially occupies the band $\left[-\frac{\pi\xi_M(\beta)}{T_\mathrm{s}}, \frac{\pi\xi_M(\beta)}{T_\mathrm{s}}\right)$ rad/s. The transmitting and receiving filters can thus be chosen as identical pulses (i.e., $g(t) = f(t)$), such that $|F(\mathrm{j}\Omega)|^2$ satisfies the T_β-Nyquist ISI-free property [35], with

$$T_\beta = \frac{T_1}{\xi_M(\beta)}, \tag{22}$$

and with frequency support $\left[-\frac{(1+\rho)\pi\xi_M(\beta)}{T_1}, \frac{(1+\rho)\pi\xi_M(\beta)}{T_1}\right)$ rad/s.

B. Faster-Than-Nyquist Transmissions

When $T_\mathrm{s} = \alpha T_1 < T_\beta = T_1/\xi_M(\beta)$, the transmissions of samples are accelerated using an FTN signaling [2]. This happens when $\alpha\xi_M(\beta) \in (0,1)$. In this case, the equivalent channel $h_{k,n}^{(\beta)}(t)$ in (5)—now with the explicit dependency on the factor β, since $(f * g)(t)$ is a T_β-Nyquist filter—accounts for the ISI induced by the fact that the Nyquist pulse assumption is no longer valid, thus potentially impacting the parameters' choice of the system, such as the guard-interval length R defined in Section II-A.

On the one hand, α should be made small to accelerate as much as possible the transmissions aiming to achieve higher data rates. On the other hand, $\alpha \leq 1$ should be made large to reduce the harmful ISI effects over the transmissions; notice also that, when there is significant ISI, bandwidth resources could also be spent in the transmission of redundant elements to cope with the underlying IBI, thus decreasing the spectral efficiency [24]. Hence, it is not straightforward to guarantee that, by decreasing α, one has spectral efficiency gains for the system model in Section II-A; nor is clear to which extent α can be decreased without significantly harming the transmission performance. These aspects will be further investigated in the next section.

C. Theoretical Analysis

Assume that $T_\mathrm{s} = \alpha T_1$ and that the discrete-time equivalent channel model of the MU-MISO system in Section II-A is parameterized by the coefficients $h_{k,n}[0]$, $h_{k,n}[1]$, …, $h_{k,n}[\nu_{\alpha,\beta}] \in \mathbb{C}$, for all $(k,n) \in \mathscr{K} \times \mathscr{N}$, wherein

$$\nu_{\alpha,\beta} \triangleq \sup_{(k,n)\in\mathscr{K}\times\mathscr{N}} \left\{\nu_0 \in \mathbb{N};\, |h_{k,n}[\nu_0]| = |h_{k,n}^{(\beta)}(\alpha\nu_0 T_1)| > \varepsilon\right\} \tag{23}$$

for a given threshold $\varepsilon \geq 0$.[2] In this case, $\nu_{\alpha,\beta}$ denotes the order of the MU-MISO channel for the sampling time $T_\mathrm{s} = \alpha T_1$ and T_β-Nyquist filter $(f * g)(t)$.

Note that, for another sampling time $T_\mathrm{s}' = \alpha' T_1$, with $\alpha' \in (0,1]$, one has $\nu_{\alpha,\beta} \approx \left(\frac{\alpha'}{\alpha}\right) \cdot \nu_{\alpha',\beta}$. As the number of redundant elements $R_{\alpha,\beta}$—now with the explicit dependency on the factors α and β—is usually proportional to $\nu_{\alpha,\beta}$ [24], [28], let us assume that $R_{\alpha,\beta} = \left\lfloor \frac{\alpha'}{\alpha} \cdot R_{\alpha',\beta} \right\rfloor$, with $\lfloor\cdot\rfloor$ standing for the floor function. Intuitively, the tendency is that when transmissions are accelerated, the channel order increases along with the corresponding guard-interval length.[3] Also, when more symbols are packed in the frequency domain (i.e., when β decreases), the effect of the underlying T_β-Nyquist filter $(f * g)(t)$ upon the physical channel $\tilde{h}_{k,n}(t)$ in (5) is to focus on a narrower channel band, thus potentially yielding discrete-time channel models with lower orders, requiring less redundant elements in the transmission.

Furthermore, consider the following definition corresponding to the achievable data rate (or maximum throughput) normalized by the bandwidth.

Definition 1: The *spectral efficiency* is

$$\mathrm{SE}_0(\alpha,\beta) \triangleq \frac{M}{M + R_{\alpha,\beta}} \cdot \frac{1}{\alpha\xi_M(\beta)} \cdot \frac{b \cdot r_\mathrm{c}}{2(1+\rho)} \quad [\mathrm{bit/s/Hz}], \tag{24}$$

in which $\xi_M(\beta)$ is defined in (21), b is the number of bits per constellation symbol, r_c is the channel coding rate, and $\rho \in (0,1]$ is the roll-off factor.

We note that Definition 1 does not take into account possible errors in the transmission/reception process.[4] With this definition, one has the following result.

Proposition 1: Given $\beta \in (0,1]$, $\mathrm{SE}_0(\alpha,\beta)$ is a decreasing function of $\alpha \in (0,1]$.

Proof: The proof is given in Appendix A. □

Remark 1: In fact, from the proof of Proposition 1, one can be more precise and state that the relative gain in the spectral efficiency that one can get from decreasing α' to α is

$$\frac{\mathrm{SE}_0(\alpha,\beta) - \mathrm{SE}_0(\alpha',\beta)}{\mathrm{SE}_0(\alpha',\beta)} \geq \left[1 - \left(\frac{\alpha}{\alpha'}\right)\right] \frac{M}{M + R_{\alpha',\beta}}. \tag{25}$$

Proposition 2: Given $\alpha \in (0,1]$, $\mathrm{SE}_0(\alpha,\beta)$ is a decreasing function of $\beta \in (0,1]$.

Proof: This follows straightforwardly from $R_{\alpha,\beta}$ being a monotonic non-increasing function of β and $\xi_M(\beta)$ being a monotonic decreasing function of β. □

Remark 2: Note that the results in Propositions 1 and 2 still hold when $R_{\alpha,\beta}$ is constant (i.e., independent of α and β). This case is also common in some practical systems that define a fixed guard-interval length based on CSI statistics, instead of optimizing it for the instantaneous CSI.

These results suggest that one should decrease T_s as much as possible or increase T_β as much as possible; yet, when doing so, the channel taps $h_{k,n}[p]$ also change (even if the physical link is kept the same). This eventually means one cannot discard the possibility of having an equivalent channel more favorable to the transmission (performance-wise, so to speak) when using, for instance, a larger T_s, which eventually might impact the *effective* spectral efficiency—the one considering transmission errors. In fact, one can already infer that the degree of acceleration is a function of the roll-off factor $\rho \in (0,1]$, considering that $|F(\mathrm{j}\Omega)|^2$ is a T_β-Nyquist pulse. Indeed, $F(\mathrm{j}\Omega)$ preserves the signal spectrum $X_n\left(\mathrm{e}^{\mathrm{j}\Omega T_\mathrm{s}}\right)$

[2]Note that $\nu_{\alpha,\beta} < \infty$ for physically meaningful channel models, otherwise one would end up with $\sum_{\nu\in\mathbb{N}} |h_{k,n}[\nu]|^2 = \infty$.

[3]In other words, in order to save bandwidth for useful data, one parsimoniously increases the amount of redundant elements—hence the use of the floor function to obtain an integer value—when accelerating the transmissions using $0 < \alpha < \alpha' \leq 1$.

[4]In Section V, we shall measure the "effective" spectral efficiency by taking into account possible errors in the transmission/reception process.

unchanged within the band $\left[-\frac{(1-\rho)\pi}{T_\beta}, \frac{(1-\rho)\pi}{T_\beta}\right)$ rad/s when $T_\mathrm{s} = T_1$, which means that virtually the transmitting pulse does not introduce frequency selectivity in the process for small ρ, as long as the signal is frequency packed by a factor β. Now, if an acceleration factor $\alpha \in (0,1)$ is employed, then the information in $X_n\left(\mathrm{e}^{\mathrm{j}\alpha\Omega T}\right)$ is within the band $\left[-\frac{\xi_M(\beta)}{\alpha}\frac{\pi}{T_1}, \frac{\xi_M(\beta)}{\alpha}\frac{\pi}{T_1}\right)$ rad/s, which means that there is an expansion of its analog frequency range. This means that part of the frequency content will be attenuated by the low-pass filter $F(\mathrm{j}\Omega)$. The smaller the value of α, the greater the induced frequency selectivity. Similarly, the smaller the value of β, the greater the induced ICI due to the loss of orthogonality among subcarriers. If α is too small, parts of the signal spectrum $X_n\left(\mathrm{e}^{\mathrm{j}\alpha\Omega T}\right)$ may be lost due to the low-pass filtering, since the output of the DAC is ideally zeroed for $|\Omega| \geq \frac{(1+\rho)\pi\xi_M(\beta)}{T_1}$. This confirms that one might accelerate the transmissions and still be able to reconstruct the signal, as long as it is above a given lower-bound, $\alpha_{\min} \in (0,1]$, for α to guarantee information losslessness [23] in the following sense.

Definition 2: The pair $(f(t), T_\mathrm{s})$ yields an *information-losslessness transmission* if, given $\tilde{x}_n(t)$ in (1), there exists a receiving filter $g(t)$ such that $\hat{x}_n[p] \triangleq \hat{x}_n(pT_\mathrm{s}) = x_n[p]$, $\forall p \in \mathscr{P}$, with $\hat{x}_n(t) \triangleq (\tilde{x}_n * g)(t)$.

The following lemma characterizes the transmitting filters that enable information-losslessness transmissions.

Lemma 1: The information-losslessness condition in Definition 2 is met if and only if

$$\sum_{i\in\mathbb{Z}} \left| F\left(\mathrm{j}\frac{(\omega+2\pi i)}{T_\mathrm{s}}\right)\right|^2 > 0, \quad \forall \omega \in \mathbb{R}. \tag{26}$$

Proof: See Lemmas 5.1 and 5.2 in [35]. □

Assuming a square-root T_β-Nyquist transmitting filter with roll-off factor $\rho \in (0,1]$, one has the following result.

Proposition 3: Given $\beta \in (0,1]$ and $M \geq 1$, one has $\alpha_{\min} = \frac{1}{(1+\rho)\xi_M(\beta)}$.

Proof: The proof is given in Appendix B. □

The next section describes how the redundancy addition/removal can deal with IBI effects.

IV. Multicarrier Symbol-Level Precoding

As explained in Section II-C, the guard interval that is usually considered for block-based transmissions might not be long enough to deal with the IBI effects stemming from accelerated signaling. As a matter of fact, even the widespread assumption that a given received data block suffers the interference from up two adjacent transmitted blocks is usually unrealistic for delay-constrained applications—i.e., those employing small to moderate block lengths $P_{\alpha,\beta} = M + R_{\alpha,\beta}$, as compared to the channel order $\nu_{\alpha,\beta}$—in which typical transmitting/receiving filters, like SRRC, are used. For this reason, we shall first propose an appropriate model for sequential transmissions, and then move on to the proposed system architecture for multicarrier SLP.

A. Sequential Transmissions

In sequential transmissions, the ℓ^{th} received block after sampling, synchronization, and buffering can be written as

$$\boldsymbol{y}_k[\ell] = \sum_{n\in\mathscr{N}} \left(\boldsymbol{H}_{\mathrm{ISI}_{k,n}} \boldsymbol{x}_n[\ell] + \sum_{b\in\mathscr{B}^{(\mathrm{f})}} \boldsymbol{H}^{(\mathrm{f})}_{\mathrm{IBI}_{k,n}}[b]\boldsymbol{x}_n[\ell-b] + \sum_{b\in\mathscr{B}^{(\mathrm{b})}} \boldsymbol{H}^{(\mathrm{b})}_{\mathrm{IBI}_{k,n}}[b]\boldsymbol{x}_n[\ell+b] \right) + \boldsymbol{v}_k[\ell], \tag{27}$$

where $\boldsymbol{x}_n[\ell] = [\, x_n[0+(\ell-1)P] \cdots x_n[P-1+(\ell-1)P]\,]^{\mathsf{T}}$, the index sets $\mathscr{B}^{(\mathrm{f})}$ and $\mathscr{B}^{(\mathrm{b})}$ contain positive integer numbers, whereas the ISI and forward/backward IBI[5] matrices are $P\times P$ Toeplitz matrices, in which, for a given group delay[6] $\delta \in \mathbb{N}$ and a given pair of row-column indexes $(p_\mathrm{r}, p_\mathrm{c}) \in \mathscr{P}^2$, one has[7]

$$\left[\boldsymbol{H}_{\mathrm{ISI}_{k,n}}\right]_{p_\mathrm{r},p_\mathrm{c}} \triangleq \begin{cases} h_{k,n}[p_\mathrm{r}-p_\mathrm{c}+\delta], & 0 \leq p_\mathrm{r}-p_\mathrm{c}+\delta \leq \nu, \\ 0, & \text{otherwise.} \end{cases} \tag{28a}$$

$$\left[\boldsymbol{H}^{(\mathrm{f})}_{\mathrm{IBI}_{k,n}}[b]\right]_{p_\mathrm{r},p_\mathrm{c}} \triangleq \begin{cases} h_{k,n}[bP+p_\mathrm{r}-p_\mathrm{c}+\delta], & 0 \leq bP+p_\mathrm{r}-p_\mathrm{c}+\delta \leq \nu, \\ 0, & \text{otherwise.} \end{cases} \tag{28b}$$

$$\left[\boldsymbol{H}^{(\mathrm{b})}_{\mathrm{IBI}_{k,n}}[b]\right]_{p_\mathrm{r},p_\mathrm{c}} \triangleq \begin{cases} h_{k,n}[-bP+p_\mathrm{r}-p_\mathrm{c}+\delta], & 0 \leq -bP+p_\mathrm{r}-p_\mathrm{c}+\delta \leq \nu, \\ 0, & \text{otherwise.} \end{cases} \tag{28c}$$

In this context, it is important to determine how many blocks affect the ℓ^{th} received block and classify them as forward and backward IBI, i.e., to characterize the index sets $\mathscr{B}^{(\mathrm{f})}$ and $\mathscr{B}^{(\mathrm{b})}$. The following result addresses this problem.

Proposition 4: Let the group delay be written as

$$\delta = q_\delta P + \rho_\delta < \nu, \tag{29}$$

with $q_\delta \in \mathbb{N}$ and $\rho_\delta \in \mathscr{P}$, and consider the integer number

$$B \triangleq \left\lceil \frac{\nu}{P} \right\rceil + 2, \tag{30}$$

with $\lceil\cdot\rceil$ standing for the ceiling function. The maximum number of blocks that may affect the reception of the ℓ^{th} data block in the sequential (streaming-like) transmission in (27) *is either*

- *B when $\rho_\delta \in \{1, 2, \ldots, \nu-(B-3)P-1\}$, or*
- *$B-1$ otherwise.*

[5]Taking ℓ as the time index of the current data block, the forward IBI corresponds to the interference coming from previous data blocks toward the current block ("$\ell-b \rightsquigarrow \ell$"), whereas the backward IBI corresponds to the interference that, for instance, the current block will generate toward previously transmitted blocks ("$\ell \rightsquigarrow \ell - b$").

[6]We employ the term "group delay" in the conventional signal processing sense, meaning the time delay of a wideband signal that is processed by a linear time-invariant filter. When working with accelerated transmissions, it is important to take into account this parameter to avoid ill-conditioned effective channel matrices.

[7]For notation clarity's sake, the dependency on α and β will be omitted in this discussion.

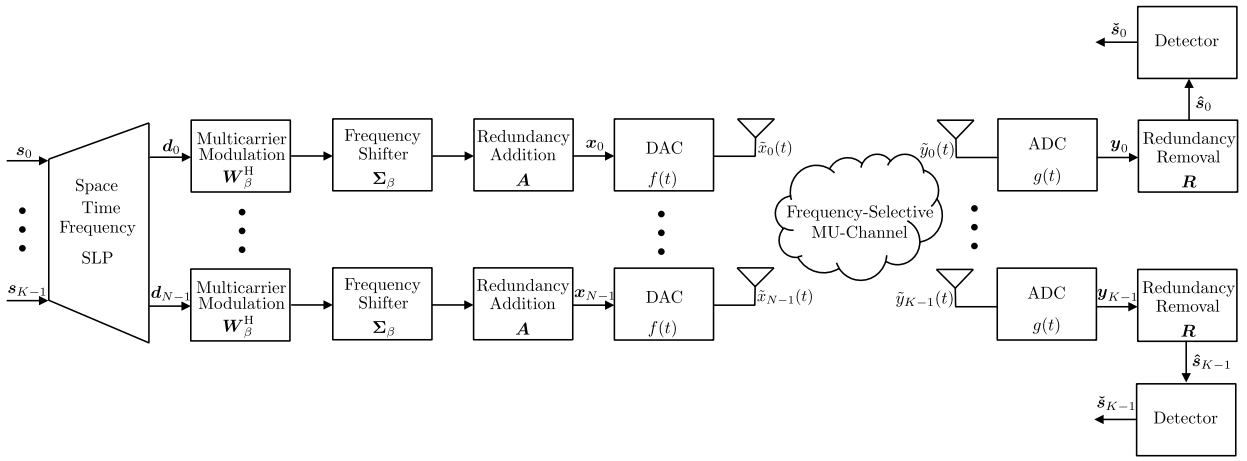

Fig. 2. Proposed multiuser MISO base-band model of a space-time-frequency symbol-level precoder.

Moreover, the index sets for the forward and backward data blocks are respectively given by

$$\mathscr{B}^{(\mathrm{f})} = \{1, \ldots, B - 2 - q_\delta\} \quad \textit{and} \quad \mathscr{B}^{(\mathrm{b})} = \{1, \ldots, q_\delta + 1\}. \tag{31}$$

Proof: The proof is given in Appendix C. □

B. Proposed System Model

We propose the multiuser system architecture depicted in Fig. 2. As compared to Fig. 1, the main differences are: (i) the amount of redundancy added at the transmitter; (ii) the way the redundancy is removed at the receiver; (iii) the absence of a multicarrier digital demodulator at the receiver; (iv) the substitution of the IDFT by the IFrFT as multicarrier modulator, followed by a frequency shifter; and (v) the use of a space-time-frequency SLP.

The primary goal of symbol-level redundancy is combating IBI. However, interference plays a twofold role in symbol-level precoders, which are able to partially benefit from constructive interference—IBI included. More specifically, considering the model in (27) and the signal-processing flow depicted in Fig. 2, as

$$\begin{aligned}\mathrm{IBI} = &\underbrace{\sum_{n\in\mathscr{N}}\sum_{b\in\mathscr{B}^{(\mathrm{f})}} \boldsymbol{R}\boldsymbol{H}^{(\mathrm{f})}_{\mathrm{IBI}_{k,n}}[b]\boldsymbol{A}\boldsymbol{\Sigma}_\beta\boldsymbol{W}_\beta^{\mathrm{H}}\boldsymbol{d}_n[\ell-b]}_{\text{forward IBI}}\\ &+\underbrace{\sum_{n\in\mathscr{N}}\sum_{b\in\mathscr{B}^{(\mathrm{b})}} \boldsymbol{R}\boldsymbol{H}^{(\mathrm{b})}_{\mathrm{IBI}_{k,n}}[b]\boldsymbol{A}\boldsymbol{\Sigma}_\beta\boldsymbol{W}_\beta^{\mathrm{H}}\boldsymbol{d}_n[\ell+b]}_{\text{backward IBI}},\end{aligned} \tag{32}$$

the forward IBI from the previous blocks is already known while designing a given block and can be used as a basis for constructive interference. However, the backward IBI of the current block toward the previous one is still destructive since the previous one has been already designed.

Thus, in order to deal with the backward IBI harmful effects, we propose the use of redundant *zero-padding zero-jamming* (ZP-ZJ) transceivers [24], [28], [30], [32], [33] with an adjustable amount of redundant elements which are added and removed through the multiplication by the matrices

$$\boldsymbol{A} \triangleq \begin{bmatrix}\boldsymbol{0}_{R_{\alpha,\beta}\times M}\\ \boldsymbol{I}_M\end{bmatrix}, \tag{33a}$$

$$\boldsymbol{R} \triangleq \begin{bmatrix}\boldsymbol{I}_M & \boldsymbol{0}_{M\times R_{\alpha,\beta}}\end{bmatrix}. \tag{33b}$$

As the amount of added redundancy has a direct impact on the spectrum efficiency of the communication system, $R_{\alpha,\beta}$ should be as small as possible. In this context, given the pair $(\boldsymbol{A}, \boldsymbol{R})$ in (33), the following result holds.

Proposition 5: The minimum guard-interval length that enables backward-IBI-free transmissions is

$$R^{\text{IBI-free}}_{\alpha,\beta} \triangleq \left\lceil \frac{\delta}{2} \right\rceil. \tag{34}$$

Proof: The proof is given in Appendix D. □

It is worth questioning whether the amount of redundant elements inserted in the transmission is reasonably small or not. In this context, consider the following definition.

Definition 3: The pair $(M, R_{\alpha,\beta})$ yields an *efficient transmission* if $M/(M + R_{\alpha,\beta}) > 50\%$.

In plain text, Definition 3 states that efficient transmissions are those where the useful data symbols in a block are more than the redundant symbols. With this definition in mind, the following result comes as a consequence of Proposition 5.

Corollary 1: For backward-IBI-free efficient transmissions one must have $\delta \in \mathscr{P}$.

Proof: For backward-IBI-free efficient transmissions one must have $2R_{\alpha,\beta} \geq \delta$ and $M > R_{\alpha,\beta}$. Thus, $P_{\alpha,\beta} = M + R_{\alpha,\beta} > R_{\alpha,\beta} + R_{\alpha,\beta} \geq \delta$. □

Remark 3: From (29) and Corollary 1, backward-IBI-free efficient transmissions are possible only when $q_\delta = 0$, which means that there is only one backward IBI block to be eliminated through the ZP-ZJ process, since $\mathscr{B}^{(\mathrm{b})} = \{1\}$.

We propose employing an adjustable reduced amount of redundant elements

$$R_{\alpha,\beta} \in \mathscr{R}_{\alpha,\beta} \triangleq \left\{0, 1, \cdots, R^{\text{IBI-free}}_{\alpha,\beta}\right\}, \tag{35}$$

which allows us to control the degree of remaining backward IBI.

Note that the pair $(\boldsymbol{A}, \boldsymbol{R})$ in (33) does not induce a circulant structure in the matrix $\boldsymbol{R}\boldsymbol{H}_{\mathrm{ISI}_{k,n}}\boldsymbol{A}$. This means that, even if a DFT matrix were to be used at the receiver side, as in

Fig. 1, no diagonalization of the effective channel matrix would be obtained. For this reason, we propose simplifying the receiver while letting the symbol-level precoder to deal with the resulting effective channel model.

The reconstructed signals $\hat{\boldsymbol{s}}_k[\ell]$ at the receiver end, $\forall k \in \mathscr{K}$, are obtained from the received block $\boldsymbol{y}_k[\ell]$ in (27) by discarding the last $R_{\alpha,\beta}$ samples of the received block, i.e., $\hat{\boldsymbol{s}}_k[\ell] = \boldsymbol{R}\boldsymbol{y}_k[\ell]$.[8] Considering the signal-processing flow depicted in Fig. 2, one can write $\boldsymbol{x}_n[\ell] = \boldsymbol{A}\boldsymbol{\Sigma}_\beta \boldsymbol{W}_\beta^{\mathrm{H}} \boldsymbol{d}_n[\ell]$, $\forall n \in \mathscr{N}$, and therefore the reconstructed signals of all users can be written as (36), shown at the bottom of the page, where the interference-plus-noise component due to the remaining backward IBI components is (37), shown at the bottom of the page.

Note that the term $\boldsymbol{H}_{\mathrm{ISI}}\boldsymbol{d}[\ell] + \sum_{b\in\mathscr{B}^{(\mathrm{f})}} \boldsymbol{H}_{\mathrm{IBI}}[b]\boldsymbol{d}[\ell-b]$ in (36) is a model for the reconstructed signal $\hat{\boldsymbol{s}}[\ell]$; the model fits perfectly the reconstructed signal in the ideal case where backward IBI and noise are not present (i.e., when $\boldsymbol{z'}[\ell] = \boldsymbol{0}$). This destructive-interference-plus-noise-free model will be used in Section IV-C for the definition of the proposed SLP scheme.

C. Non-Linear Space-Time-Frequency Symbol-Level Precoder

We propose using a space-time-frequency SLP scheme accounting for MUI and frequency-selective-related interference—in the form of ISI, ICI, and IBI. The idea is to exploit the interference in space, time, and frequency domains in a constructive manner. Inspired by the *dirty paper coding* (DPC) principle [36], the knowledge of the forward IBI $\sum_{b\in\mathscr{B}^{(\mathrm{f})}} \boldsymbol{H}_{\mathrm{IBI}}[b]\boldsymbol{d}[\ell-b]$ can be taken into account in the transmission, whereas the remaining backward IBI in $\boldsymbol{z'}[\ell]$ tends to degrade the system performance.

A possible cost function is related to the minimization of total transmit power. If only one block were to be transmitted as in (1), then the corresponding total energy (i.e., considering all transmit antennas) would be

$$E \triangleq \sum_{n\in\mathscr{N}} \int_{-\infty}^{\infty} \frac{|\tilde{x}_n(t)|^2}{Z_0}\mathrm{d}t = \tfrac{1}{Z_0}\textstyle\sum_{n\in\mathscr{N}} \boldsymbol{x}_n^{\mathrm{H}}\boldsymbol{C}_f\boldsymbol{x}_n, \tag{38}$$

in which $Z_0 > 0$ denotes the antenna impedance, $|\tilde{x}_n(t)|^2/Z_0$ is the instantaneous power, and $[\boldsymbol{C}_f]_{p_\mathrm{r},p_\mathrm{c}} \triangleq (f * f)\left((p_\mathrm{r}-p_\mathrm{c})T_\mathrm{s}\right)$, for all $p_\mathrm{r}, p_\mathrm{c} \in \mathcal{P}$. As mentioned before, $f(t)$ is assumed to be a square-root T_β-Nyquist filter with even symmetry around the origin $t = 0$. Since $T_\mathrm{s} \neq T_\beta$ in general, then the temporal correlations of the transmitting pulse must be taken into account when modeling the transmission power, which is proportional to the total energy.

Once again, recalling that $\boldsymbol{x}_n = \boldsymbol{A}\boldsymbol{\Sigma}_\beta\boldsymbol{W}_\beta^{\mathrm{H}}\boldsymbol{d}_n$ (see Fig. 2), one can rewrite (38) as (39), shown at the bottom of the next page, and therefore, by using the model for the reconstructed signal (cf. the end of Section IV-B), the proposed SLP *convex* optimization problem is[9]

$$\begin{aligned} &\underset{\boldsymbol{d}[\ell]\in\mathbb{C}^{NM\times 1}}{\text{minimize}} \ \boldsymbol{d}^{\mathrm{H}}[\ell]\boldsymbol{\Gamma}\boldsymbol{d}[\ell] \\ &\text{subject to } \boldsymbol{H}_{\mathrm{ISI}}\boldsymbol{d}[\ell] + \sum_{b\in\mathscr{B}^{(\mathrm{f})}} \boldsymbol{H}_{\mathrm{IBI}}[b]\boldsymbol{d}[\ell-b] \succeq \boldsymbol{q}\odot\boldsymbol{s}[\ell], \end{aligned} \tag{40}$$

[8] From the reconstructed signals $\hat{\boldsymbol{s}}_k[\ell]$ one can detect the symbols by means of a conventional single-user hard or soft detection, or directly reconstruct the bits using hard or soft decoding schemes.

[9] The problem is strictly convex, since $\boldsymbol{\Gamma}$ is a positive-definite matrix. One can use the CVX software [37] to solve such a problem.

$$\begin{aligned} \underbrace{\begin{bmatrix}\hat{\boldsymbol{s}}_0[\ell]\\ \vdots \\ \hat{\boldsymbol{s}}_{K-1}[\ell]\end{bmatrix}}_{\triangleq\hat{\boldsymbol{s}}[\ell]} &= \underbrace{\begin{bmatrix}\boldsymbol{R}\boldsymbol{H}_{\mathrm{ISI}_{0,0}}\boldsymbol{A}\boldsymbol{\Sigma}_\beta\boldsymbol{W}_\beta^{\mathrm{H}} & \cdots & \boldsymbol{R}\boldsymbol{H}_{\mathrm{ISI}_{0,N-1}}\boldsymbol{A}\boldsymbol{\Sigma}_\beta\boldsymbol{W}_\beta^{\mathrm{H}} \\ \vdots & \ddots & \vdots \\ \boldsymbol{R}\boldsymbol{H}_{\mathrm{ISI}_{K-1,0}}\boldsymbol{A}\boldsymbol{\Sigma}_\beta\boldsymbol{W}_\beta^{\mathrm{H}} & \cdots & \boldsymbol{R}\boldsymbol{H}_{\mathrm{ISI}_{K-1,N-1}}\boldsymbol{A}\boldsymbol{\Sigma}_\beta\boldsymbol{W}_\beta^{\mathrm{H}}\end{bmatrix}}_{\triangleq\boldsymbol{H}_{\mathrm{ISI}}\in\mathbb{C}^{KM\times NM}} \underbrace{\begin{bmatrix}\boldsymbol{d}_0[\ell]\\ \vdots \\ \boldsymbol{d}_{N-1}[\ell]\end{bmatrix}}_{\triangleq\boldsymbol{d}[\ell]} \\ &\quad + \sum_{b\in\mathscr{B}^{(\mathrm{f})}} \underbrace{\begin{bmatrix}\boldsymbol{R}\boldsymbol{H}^{(\mathrm{f})}_{\mathrm{IBI}_{0,0}}[b]\boldsymbol{A}\boldsymbol{\Sigma}_\beta\boldsymbol{W}_\beta^{\mathrm{H}} & \cdots & \boldsymbol{R}\boldsymbol{H}^{(\mathrm{f})}_{\mathrm{IBI}_{0,N-1}}[b]\boldsymbol{A}\boldsymbol{\Sigma}_\beta\boldsymbol{W}_\beta^{\mathrm{H}} \\ \vdots & \ddots & \vdots \\ \boldsymbol{R}\boldsymbol{H}^{(\mathrm{f})}_{\mathrm{IBI}_{K-1,0}}[b]\boldsymbol{A}\boldsymbol{\Sigma}_\beta\boldsymbol{W}_\beta^{\mathrm{H}} & \cdots & \boldsymbol{R}\boldsymbol{H}^{(\mathrm{f})}_{\mathrm{IBI}_{K-1,N-1}}[b]\boldsymbol{A}\boldsymbol{\Sigma}_\beta\boldsymbol{W}_\beta^{\mathrm{H}}\end{bmatrix}}_{\triangleq\boldsymbol{H}_{\mathrm{IBI}}[b]\in\mathbb{C}^{KM\times NM}} \begin{bmatrix}\boldsymbol{d}_0[\ell-b]\\ \vdots \\ \boldsymbol{d}_{N-1}[\ell-b]\end{bmatrix} \\ &\quad + \underbrace{\begin{bmatrix}\boldsymbol{z'}_0[\ell]\\ \vdots \\ \boldsymbol{z'}_{K-1}[\ell]\end{bmatrix}}_{\triangleq\boldsymbol{z'}[\ell]} \\ &= \boldsymbol{H}_{\mathrm{ISI}}\boldsymbol{d}[\ell] + \sum_{b\in\mathscr{B}^{(\mathrm{f})}} \boldsymbol{H}_{\mathrm{IBI}}[b]\boldsymbol{d}[\ell-b] + \boldsymbol{z'}[\ell], \end{aligned} \tag{36}$$

$$\boldsymbol{z'}[\ell] = \sum_{b\in\mathscr{B}^{(\mathrm{b})}} \begin{bmatrix}\boldsymbol{R}\boldsymbol{H}^{(\mathrm{b})}_{\mathrm{IBI}_{0,0}}[b]\boldsymbol{A}\boldsymbol{\Sigma}_\beta\boldsymbol{W}_\beta^{\mathrm{H}} & \cdots & \boldsymbol{R}\boldsymbol{H}^{(\mathrm{b})}_{\mathrm{IBI}_{0,N-1}}[b]\boldsymbol{A}\boldsymbol{\Sigma}_\beta\boldsymbol{W}_\beta^{\mathrm{H}} \\ \vdots & \ddots & \vdots \\ \boldsymbol{R}\boldsymbol{H}^{(\mathrm{b})}_{\mathrm{IBI}_{K-1,0}}[b]\boldsymbol{A}\boldsymbol{\Sigma}_\beta\boldsymbol{W}_\beta^{\mathrm{H}} & \cdots & \boldsymbol{R}\boldsymbol{H}^{(\mathrm{b})}_{\mathrm{IBI}_{K-1,N-1}}[b]\boldsymbol{A}\boldsymbol{\Sigma}_\beta\boldsymbol{W}_\beta^{\mathrm{H}}\end{bmatrix} \begin{bmatrix}\boldsymbol{d}_0[\ell+b]\\ \vdots \\ \boldsymbol{d}_{N-1}[\ell+b]\end{bmatrix} + \begin{bmatrix}\boldsymbol{R}\boldsymbol{v}_0[\ell]\\ \vdots \\ \boldsymbol{R}\boldsymbol{v}_{K-1}[\ell]\end{bmatrix}. \tag{37}$$

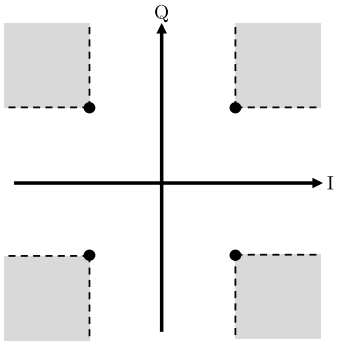

Fig. 3. QPSK constellation (symbols in black big dots) with the corresponding CI regions (in gray).

in which $\boldsymbol{s}[\ell] \in \mathbb{C}^{KM\times 1}$ contains the actual intended symbols for all K users, $\boldsymbol{q} \in \mathbb{C}^{KM\times 1}$ collects quality-of-service-related parameters, such as target *signal-to-interference-plus-noise ratio* (SINR) $\gamma_k > 0$ and noise variance $\sigma_k^2 > 0$, with $k \in \mathscr{K}$, and $\odot$ denotes point-wise product between vectors. The operator $\trianglerighteq$ denotes that each entry of the vector in the L.H.S. of the constraint in (40)—i.e., the model for the clean reconstructed signals—belongs to the *constructive interference* (CI) region of the corresponding intended symbol in the vector $\boldsymbol{s}[\ell]$, as explained below. The constraint in (40) is responsible for shaping the precoded signals so that the corresponding communication signals are added constructively at the receiver end.

Fig. 3 illustrates the CI regions for a QPSK constellation. As an example, assume that the intended symbol for the k^{th} user at the m^{th} subcarrier of the ℓ^{th} block is $s_k[m+(\ell-1)M] = (1+\mathrm{j})/\sqrt{2}$, i.e., the black big dot in the first quadrant of Fig. 3. Then, having the corresponding reconstructed signal $\hat{s}_k[m+(\ell-1)M]$ with $\Re\{\hat{s}_k[m+(\ell-1)M]\} \geq q_k/\sqrt{2}$ and $\Im\{\hat{s}_k[m+(\ell-1)M]\} \geq q_k/\sqrt{2}$ means that constructive interference has taken place. Indeed, in this example, the reconstructed signal $\hat{s}_k[m+(\ell-1)M]$ belongs to the unlimited gray region in the first quadrant of Fig. 3, which means it has been pushed further deeper into the proper decision region of the scaled constellation symbol $q_k \cdot s_k[m+(\ell-1)M]$—the scaling factor $q_k = \sigma_k\sqrt{\gamma_k}$ guarantees that the desired quality-of-service is satisfied for the k^{th} user. Hence, for a QPSK constellation and for each $(m,k) \in \mathscr{M}\times\mathscr{K}$, one can define $m_\ell \triangleq m+(\ell-1)M$ so that the constraint in (40) can be detailed as follows (41), shown at the bottom of the page.

The above discussion exemplifies how to define the operator $\trianglerighteq$ related to the CI regions of a given constellation. Such definition can be generalized to higher-order constellations. Since this generalization has been extensively described in the literature [9]–[11], [13], [38]–[40], we shall omit further details on it. In all cases, the operator $\trianglerighteq$ defines a convex set.

While channel-level precoding techniques (e.g., the scheme described in Section II or the MU-MISO-SEFDM scheme proposed in [21]) deal with interference as an undesired received signal component that should therefore be suppressed—for instance, by targeting the exact constellation symbols (black big dots in Fig. 3)—, SLP approaches interference by manipulating it in such a way that it constructively contributes to the desired signal of each user. This simultaneously confers more degrees of freedom for minimizing the total transmit power—directly related to the cost function in (40)—, while also enhances the detection performance, since the clean reconstructed signals are placed farther apart from the decision boundaries, allowing for stronger perturbations. These advantages come at a price of higher computational burden.

The aforementioned high computational complexity stems from two reasons. Firstly, the term "symbol level" refers to the fact that in order to induce and exploit CI, one needs to redesign the precoder for each new symbol vector $\boldsymbol{s}[\ell]$. This is in contrast to channel-level precoding that requires redesigning of the precoder only when the effective CSI is updated, which happens less often than the MC-symbol rate either due to changes in the physical channel or to modifications in the frequency-packing FTN parameters. Secondly, computing the precoded vectors is more complex for SLP, since those vectors are the solutions—through iterative numerical processes—to the optimization problem in (40), whereas linear channel-level

$$
\begin{aligned}
Z_0E &= \sum_{n\in\mathscr{N}} \boldsymbol{d}_n^{\mathrm{H}}\boldsymbol{W}_\beta\boldsymbol{\Sigma}_\beta^*\boldsymbol{A}^{\intercal}\boldsymbol{C}_f\boldsymbol{A}\boldsymbol{\Sigma}_\beta\boldsymbol{W}_\beta^{\mathrm{H}}\boldsymbol{d}_n \\
&= \begin{bmatrix}\boldsymbol{d}_0^{\mathrm{H}} & \cdots & \boldsymbol{d}_{N-1}^{\mathrm{H}}\end{bmatrix} \underbrace{\begin{bmatrix}\boldsymbol{W}_\beta\boldsymbol{\Sigma}_\beta^*\boldsymbol{A}^{\intercal}\boldsymbol{C}_f\boldsymbol{A}\boldsymbol{\Sigma}_\beta\boldsymbol{W}_\beta^{\mathrm{H}} & & \\ & \ddots & \\ & & \boldsymbol{W}_\beta\boldsymbol{\Sigma}_\beta^*\boldsymbol{A}^{\intercal}\boldsymbol{C}_f\boldsymbol{A}\boldsymbol{\Sigma}_\beta\boldsymbol{W}_\beta^{\mathrm{H}}\end{bmatrix}}_{=\boldsymbol{I}_N\otimes\left(\boldsymbol{W}_\beta\boldsymbol{\Sigma}_\beta^*\boldsymbol{A}^{\intercal}\boldsymbol{C}_f\boldsymbol{A}\boldsymbol{\Sigma}_\beta\boldsymbol{W}_\beta^{\mathrm{H}}\right)\triangleq\boldsymbol{\Gamma}\in\mathbb{C}^{NM\times NM}} \begin{bmatrix}\boldsymbol{d}_0\\ \vdots \\ \boldsymbol{d}_{N-1}\end{bmatrix} \\
&= \boldsymbol{d}^{\mathrm{H}}\boldsymbol{\Gamma}\boldsymbol{d},
\end{aligned} \tag{39}
$$

$$
\left[\Re\left\{\boldsymbol{H}_{\mathrm{ISI}}\boldsymbol{d}[\ell] + \sum_{b\in\mathscr{B}^{(\mathrm{f})}}\boldsymbol{H}_{\mathrm{IBI}}[b]\boldsymbol{d}[\ell-b]\right\}\right]_{(m_\ell+kM)} \underset{\Re\{s_k[m_\ell]\}<0}{\overset{\Re\{s_k[m_\ell]\}>0}{\gtrless}} q_k\Re\{s_k[m_\ell]\}, \tag{41a}
$$

$$
\left[\Im\left\{\boldsymbol{H}_{\mathrm{ISI}}\boldsymbol{d}[\ell] + \sum_{b\in\mathscr{B}^{(\mathrm{f})}}\boldsymbol{H}_{\mathrm{IBI}}[b]\boldsymbol{d}[\ell-b]\right\}\right]_{(m_\ell+kM)} \underset{\Im\{s_k[m_\ell]\}<0}{\overset{\Im\{s_k[m_\ell]\}>0}{\gtrless}} q_k\Im\{s_k[m_\ell]\}. \tag{41b}
$$

precoding has its complexity defined by conventional matrix-vector multiplications.

The precise computational complexity of the proposed SLP approach depends on the specific iterative algorithm employed to solve problem (40). An efficient way to solve it is to use the accelerated projected gradient descent algorithm [41] and the resulting computational complexity is (cf. Section 4.5 of [40] for further details)

$$\begin{aligned}\#\text{FLOPs} = {} & 24NK^2M^3 + 16K^3M^3 + 12NKM^2 \\ & - 2K^2M^2 - 3KM + \left(8K^2M^2 + 6KM\right)\left\lceil \frac{1}{\sqrt{\epsilon}} \right\rceil,\end{aligned} \tag{42}$$

where the parameter $\epsilon > 0$ defines the accuracy of the solution with respect to the actual optimal point. The above complexity is much higher than, for instance, the complexity for implementing (13), which is $\#\text{FLOPs} = 2NKM - NM$. On the one hand, the higher computational burden of the proposal impacts the base-station, which tends to be a much more computationally powerful unit; on the other hand, the receiver processing is actually simplified as compared to the ZF scheme described in Section II or the MU-MISO-SEFDM [21].

V. Numerical Results

The performance of the proposed space-time-frequency symbol-level precoders is assessed via four experiments. The first one focuses on a conventional multicarrier signaling without neither frequency packing nor FTN capabilities; the main objective of this experiment is to compare the proposed SLP approach against the conventional OFDM-based linear ZF precoder for multipath-fading channels across different number of users. The second experiment focuses on channel-coded frequency-packed multicarrier signaling over flat-fading channels across different SINRs; the main goal here is to benchmark the proposal against the state-of-the-art MU-MISO-SEFDM scheme proposed in [21]. The third numerical experiment focuses on frequency-packed FTN multicarrier signaling over flat-fading channels across different SINRs; the main objective here is to explore the underlying trade-offs while varying the acceleration and packing factors, α and β respectively, in terms of data rate, transmit power, as well as to showcase the interplay between spectral and energy efficiencies. The forth experiment focuses on frequency-packed FTN multicarrier signaling over multipath-fading channels across different values of α and β. The main goal here is to verify some of the theoretical predictions regarding α and β in a realistic scenario.

For all experiments, the transmitting/receiving filters are T_β-SRRC pulses, for a fixed basic Nyquist period $T_1 = 100$ ns, and with roll-off factor $\rho = 1/4$ for Experiments 1, 3, and 4, or $\rho = 1/10$ for Experiment 2. The additive noise is white Gaussian with variance fixed at $\sigma^2 = 1$, and the antenna impedance employed for power calculations is $Z_0 = 50\ \Omega$.

The figures of merit are:

(i) *effective sum rate (or throughput)* given by $\text{SR} \triangleq K \cdot \frac{M}{P} \cdot \frac{b}{T_\text{s}} \cdot (1 - \text{SER})$ [bit/s], in which $\text{SER} \triangleq \frac{1}{K}\sum_{k\in\mathscr{K}} \text{SER}^{(k)}$ is the average *symbol error rate* and b is the number of bits per constellation symbol.

(ii) *time-averaged total transmit power*, $\mathbb{P}_\text{t}$, computed as the total analog power [W] feeding the transmitting antennas averaged over the interval PT_s. Here we consider the actual analog power including the cross-power terms resulting from the sequential block-based transmission.

(iii) *effective system spectral efficiency*, $\text{SE} \triangleq \frac{\text{SR}}{\text{BW}}$ [bit/s/Hz], wherein $\text{BW} \triangleq \frac{2(1+\rho)}{T_\beta}$ is the bandwidth of the base-band transmitted signal.

(iv) *channel-coded bit-error rate*, named Coded BER.

(v) *overall energy inefficiency*, $\text{EI} \triangleq \frac{\mathbb{P}_\text{t}}{\text{SE}}$ [J/bit].

Note that all figures of merit take into account the added redundancy.

A. Experiment 1

We first study the performance of the proposed SLP approach with respect to different number of users $K \in \{4, \ldots, N\}$, for a downlink transmission using $N = 8$ antennas. In this experiment, no frequency-packed FTN signaling is considered, i.e., $(\alpha, \beta) = (1, 1)$. The number of subcarriers is fixed at $M = 64$, the constellation $\mathcal{C}$ is 16-QAM, and the base-band multipath-fading models correspond to Rayleigh channels with exponentially decaying power profile and with resulting order varying around $\nu = 24$. As there is no time acceleration ($\alpha = 1$), $\delta = 0$ yielded well-conditioned effective channel matrices. The quality of service vector is $\boldsymbol{q} = \sqrt{\gamma\sigma^2}\mathbf{1}_{KM\times 1}$, where the target SINR γ corresponds to 15 dB. The guard-interval length is chosen as: (i) $R = 0$, called 'No red. SLP' for the proposed space-time-frequency SLP,[10] and (ii) $R = \nu$, called 'Full red. ZF', for the baseline ZF precoder using full redundancy, which is able to both eliminate IBI and induce a circulant effective channel matrix.

Fig. 4 depicts the results. Fig. 4(a) lets clear that the proposed SLP scheme outperforms the ZF precoder in terms of effective sum rate. Note that the IBI had no harmful effect whatsoever on the non-redundant precoder. The scenario with a higher number of users tends to be more challenging, but the SLP is able to gain more with the interference exploitation. For $K = 8$, the throughput gap drops a bit at the cost of a much higher transmit power for the ZF precoder. Indeed, Fig. 4(b) shows that, although the ZF precoder requires slightly less transmit power than the proposed SLP for $K \leq 7$, it requires much more power in a fully-loaded system ($K = N = 8$). Fig. 4(c) shows the superior performance of the proposed SLP when both spectral and energy efficiencies are taken into account for all considered $K \in \{4, \ldots, N\}$.

B. Experiment 2

We now benchmark the proposed SLP approach against the state-of-the-art technique for MU-MISO frequency-packed MC signaling proposed in [21]. We consider the same setup for which the MU-MISO-SEFDM scheme [21] was originally devised, namely: frequency-packed MC signaling (i.e., $\alpha = 1$ and $\beta < 1$) over flat-fading channels. This benchmark comprises a two-stage waveform and space precoding architecture. The waveform precoding pre-equalizes the self-created ICI within the waveform due to frequency-packing, whereas

[10] Since $\delta = 0$, one has $\mathscr{R}_{\alpha,\beta} = \{0\}$ in (35).

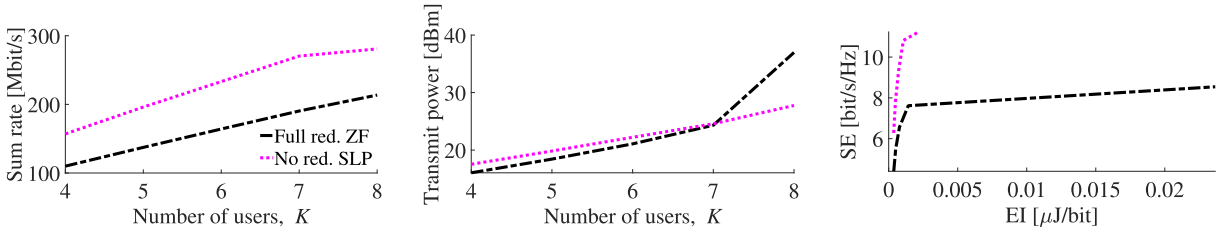

(a) Effective sum rate. (b) Time-averaged total transmit power. (c) Spectral efficiency *vs.* energy inefficiency for $K \in \{4, \ldots, 8\}$.

Fig. 4. (*Experiment 1*) Performance comparison between the ZF precoder with full redundancy and the proposed space-time-frequency SLP with no redundancy, as function of K and for $(\alpha, \beta) = (1, 1)$. The legend in (a) applies to all figures.

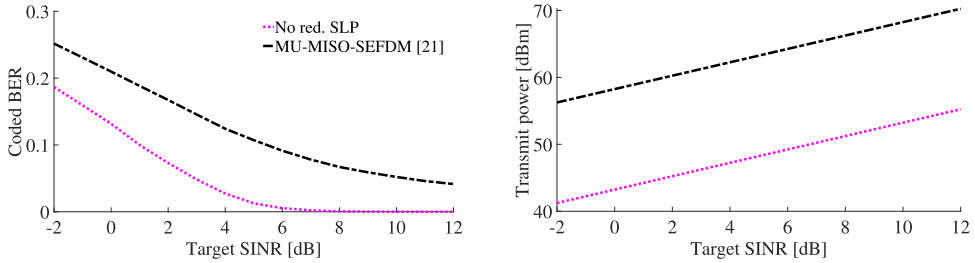

(a) Channel-coded bit-error rate. (b) Time-averaged total transmit power.

Fig. 5. (*Experiment 2*) Performance comparison between the proposed space-time-frequency non-redundant SLP and the baseline scheme MU-MISO-SEFDM [21]. The legend in (a) applies to both figures.

the space precoding pre-cancels the spatial MUI. We consider delay-constrained applications with a short multicarrier-symbol duration (i.e., with a small number of subcarriers, $M = 16$) for a QPSK constellation, in a fully-loaded system with $N = K = 4$. In addition, we use a Reed-Solomon error correction scheme with parameters $(8, 4)$ in the Galois field GF(2^4). This choice of parameters stems from the option to encode each multicarrier symbol separately.[11] In order to get maximum packing capability, the frequency-packing factor β is set as small as possible while satisfying the theoretical bound in Proposition 3, i.e., $\beta \approx 0.9093$, which represents about 10% of bandwidth savings. In this comparison, we consider only the 'No red. SLP' across different SINR values.

Fig. 5 depicts the results. It is clear that the proposed SLP scheme outperforms the benchmark in terms of both channel-coded BER and total transmit power. Note that the IBI had no harmful effect whatsoever on the non-redundant precoder. This significant performance enhancement comes at a cost of entailing a higher computational burden for precoding the signals at the base-station, since the benchmark from [21] is a channel-level linear precoder, whereas our proposal is a symbol-level non-linear precoder.

C. Experiment 3

We now address the following questions: Is it really necessary to use frequency-packed FTN? Why not simply increasing the constellation size (e.g., from QPSK to 8PSK)? What are the trade-offs when we change the parameters α and β? In order to answer these questions, we study the SLP performance for frequency-packed FTN transmissions over flat-fading channels. Once again, we consider $M = 16$ in a fully-loaded system with $N = K = 4$, but now for both QPSK as well as 8PSK constellations.

For the sake of clarity, we consider only the 'No red. SLP' for different values of α and β. More specifically, $(\alpha, \beta) \in \{(0.90, 0.88), (0.80, 1), (1, 0.79), (1, 1)\}$.[12]

Fig. 6 depicts the results. Fig. 6(a) shows that, as expected, if we jump from QPSK to 8PSK with no frequency packed FTN signaling, i.e. with $(\alpha, \beta) = (1, 1)$, we can obtain higher spectral efficiency at a cost of lower energy efficiency (i.e., higher energy inefficiency). There is a region in the SE $\times$ EI plane, however, where it is better to use QPSK rather than 8PSK. This happens for sufficiently small target SINR. On the other hand, when $\alpha < 1$ or $\beta < 1$, we find a region in the SE $\times$ EI plane where it is better to use frequency packing and/or FTN signaling as compared to not using it. For example, at EI $= 0.6$ nJ/bit, there is about 12% improvement in the SE when $\alpha < 1$ and/or $\beta < 1$ as compared to a QPSK transmission with $(\alpha, \beta) = (1, 1)$. Again, this holds for sufficiently small target SINR, since one can get higher spectral efficiency with 8PSK without packing nor acceleration with the same energy efficiency of the other techniques for sufficiently large target SINRs. Fig. 6(a) also lets clear the equivalence among the different techniques with $\alpha < 1$ and/or $\beta < 1$ in the SE $\times$ EI plane. The same virtual equivalence is observed in terms of SER performance[13] in Fig. 6(b); but

[11] Considering $M = 16$ QPSK symbols, each multicarrier symbol comprises 32 bits ($= 8 \times 4$) for each codeword; the codewords are associated with 16-bit ($= 4 \times 4$) messages, resulting in $r_c = 1/2$.

[12] Note that, when $(\alpha, \beta) \in \{(0.90, 0.88), (0.80, 1), (1, 0.79)\}$, one has $\alpha \cdot \xi_M(\beta) \approx \frac{1}{1+\rho}$; see also Proposition 3.

[13] Note that when $\alpha < 1$ and/or $\beta < 1$ the SER reaches a floor value as the SINR increases. This stems from the destructive effect of the backward IBI that is not eliminated by the non-redundant ($R_{\alpha,\beta} = 0$) SLP scheme. Note that, when $(\alpha, \beta) = (1, 1)$, there is no IBI (keep in mind that in this experiment we consider flat-fading channels) and the SER tends to zero as the SINR grows. One could decrease the SER floor level down to zero by increasing $R_{\alpha,\beta}$.

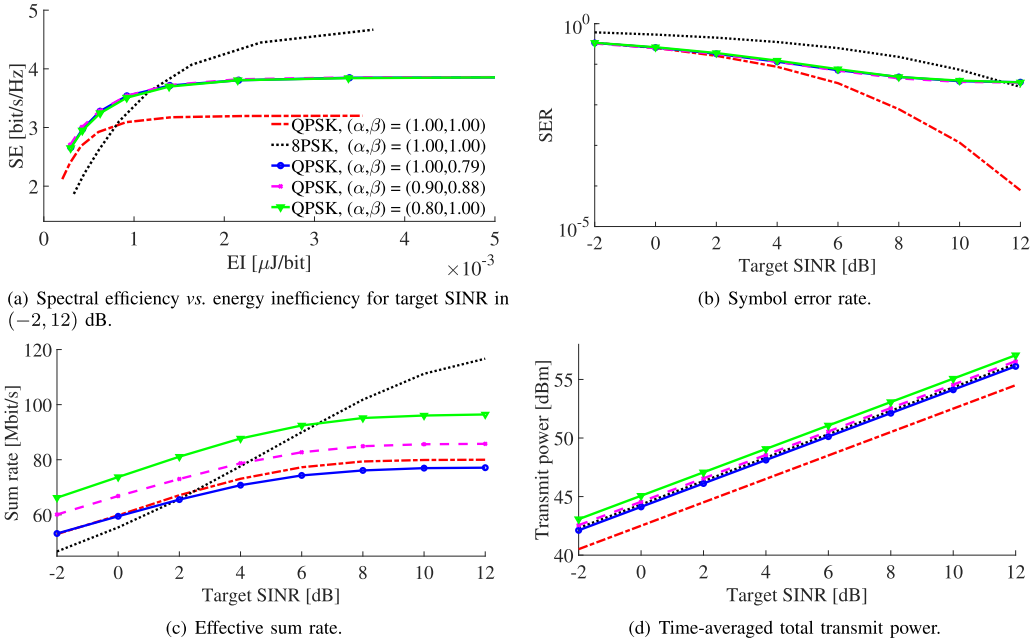

(a) Spectral efficiency *vs.* energy inefficiency for target SINR in $(-2, 12)$ dB.

(b) Symbol error rate.

(c) Effective sum rate.

(d) Time-averaged total transmit power.

Fig. 6. (*Experiment 3*) Performance comparison between different versions of the proposed space-time-frequency non-redundant SLP across different target SINR values. The legend in (a) applies to all figures.

these techniques differ in other figures of merit, as explained in the following discussion.

Fig. 6(c) shows that the effective sum rate of the accelerated schemes ($\alpha < 1$) is superior than the non-accelerated ones. For example, at SINR $= 4$ dB, there is about 20% improvement in the effective sum rate when $(\alpha, \beta) = (0.80, 1)$ and about 8% improvement when $(\alpha, \beta) = (0.90, 1)$, as compared to a QPSK transmission with $(\alpha, \beta) = (1, 1)$. It is interesting to note that the frequency-packed non-accelerated transmission with $(\alpha, \beta) = (1, 0.79)$ achieves virtually the same throughput of the QPSK with $(\alpha, \beta) = (1, 1)$ but using only $\xi_M(\beta) \approx 80\%$ of its bandwidth. Fig. 6(d) shows that the technique that requires more transmit power is the one with $(\alpha, \beta) = (0.80, 1)$, which partially explains from where it comes its outstanding throughput performance. We therefore note that, although the techniques with $\alpha < 1$ and/or $\beta < 1$ are virtually equivalent in the SE $\times$ EI plane, there is a trade-off among bandwidth usage, transmit power consumption, and throughput; this trade-off is controlled by the parameters α and β, which confer added flexibility to the system designer.

D. Experiment 4

We now study the SLP performance for FTN signaling with and without frequency packing and our main goal is to verify the theoretical prediction in Proposition 3. We consider $M = 32$ subcarriers, $N = 4$ transmitting antennas, $K = N$ users, a QPSK constellation, and a target SINR γ of 6 dB. Besides the baseline ZF linear precoder with full redundancy $R = \nu$, two space-time-frequency SLP precoders are employed according to the following guard-interval lengths: (i) $R = \lceil \frac{\delta}{4} \rceil$, called 'Quarter-delay red. SLP' and (ii) $R = \lceil \frac{\delta}{2} \rceil$, called 'Half-delay red. SLP'. In the simulations, we consider multipath-fading physical channels and the resulting effective channel order ν was around 25, whereas the group delay δ was around 10, depending on the specific values of α and β. We consider $\beta \in \{0.80, 0.90, 1\}$. According to Proposition 3, for each value of β, one has a specific value for $\alpha_{\min}$; in this case, $\alpha_{\min} \in \{0.99, 0.89, 0.80\}$. We therefore chose a range of values for α according to these minimum values.[14]

Fig. 7 depicts the spectral efficiency results. First of all, notice that the ZF precoder is quite inefficient since it is spending too much bandwidth resources with redundant signals (guard interval) that do not carry information. The proposed redundant precoder with $R = \lceil \delta/4 \rceil$ attains the highest spectral efficiency among the tested schemes. The peak of the spectral efficiency is always achieved at the point $\alpha = \alpha_{\min}$. From Fig. 7(b), one can see that the SE increases about 25% (for $R = \lceil \delta/2 \rceil$) and 22% (for $R = \lceil \delta/4 \rceil$) at $\alpha = \alpha_{\min}$, as compared to the SE value obtained for non-accelerated transmissions (i.e., $\alpha = 1$). From Fig. 7(c), one can see that the SE improves about 11% (for $R = \lceil \delta/2 \rceil$) and 16% (for $R = \lceil \delta/4 \rceil$) at $\alpha = \alpha_{\min}$ when compared to $\alpha = 1$. It is worth mentioning that the spectral efficiency enhancement of the proposed SLP when compared to the baseline scheme comes at a price of higher computational burden.

Fig. 8 shows the energy inefficiency results. The proposed redundant precoders are the most energy efficient ones, wherein the minimum-redundancy scheme with $R = \lceil \delta/2 \rceil$ attains the highest energy efficiency (lowest inefficiency). Looking at the ZF curves, one can see that when trying to accelerate below the minimum value of α that guarantees information losslessness, the scheme starts to spend significantly more transmit power without having gains in spectral efficiency (see Fig. 7). Although less noticeable in this particu-

[14]Unfortunately, it was not possible to go much below the minimum value of α that guarantees information losslessness without facing some numerical issues, which limited the range of values that could be tested for the acceleration factor.

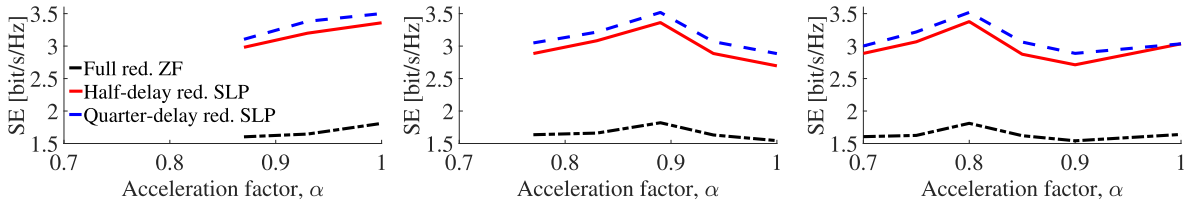

(a) $\beta = 0.80$ and $\alpha_{\min} \approx 0.99$. (b) $\beta = 0.90$ and $\alpha_{\min} \approx 0.89$. (c) $\beta = 1.00$ and $\alpha_{\min} = 0.80$.

Fig. 7. (*Experiment 4*) Spectral efficiency comparison between the ZF precoder with full redundancy and the proposed space-time-frequency SLPs with half-delay ($\lceil \delta/2 \rceil$) and quarter-delay ($\lceil \delta/4 \rceil$) redundancies, as function of α and for $\beta = 1$. The legend in (a) applies to all figures.

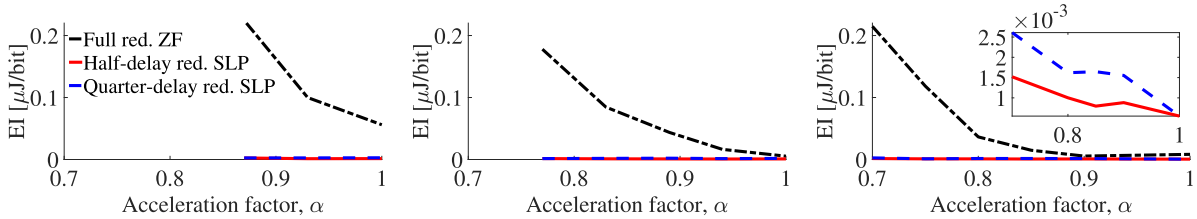

(a) $\beta = 0.80$ and $\alpha_{\min} \approx 0.99$. (b) $\beta = 0.90$ and $\alpha_{\min} \approx 0.89$. (c) $\beta = 1.00$ and $\alpha_{\min} = 0.80$.

Fig. 8. (*Experiment 4*) Energy inefficiency comparison between the ZF precoder with full redundancy and the proposed space-time-frequency SLPs with half-delay ($\lceil \delta/2 \rceil$) and quarter-delay ($\lceil \delta/4 \rceil$) redundancies, as function of α and for different values of β. The legend in (a) applies to all figures.

TABLE I

(*Experiment 4*) SER OF THE PROPOSED REDUNDANT SPACE-TIME-FREQUENCY SLPS

(α, β)	$R = \lceil \delta/4 \rceil$	$R = \lceil \delta/2 \rceil$
$(1.00, 0.80)$	4.92%	2.98%
$(0.89, 0.90)$	4.76%	3.47%
$(0.80, 1.00)$	5.46%	4.52%

lar experiment, the same behavior is observed for the proposed non-redundant systems.

Table I shows a numerical comparison of the SER corresponding to the peak values of SE in Fig. 7 for the proposed redundant SLPs. As expected, one can clearly notice that the SER decreases when R increases.

VI. CONCLUDING REMARKS

This paper addressed the problem of jointly handling multiuser, intersymbol, and intercarrier interference in downlink multi-antenna multicarrier transmissions through frequency-selective channels. More specifically, controlled intersymbol and intercarrier interference were introduced via frequency-packed faster-than-Nyquist signaling. In this context, redundant block-based space-time-frequency symbol-level precoding schemes were proposed. The introduction of redundancy in the block-based transmissions achieved a trade-off between constructive and destructive interference effects at the user terminals. A complete characterization of the *interblock interference* (IBI), taking into account that the resulting effective channel models can generate interference across many multicarrier symbols (not only two adjacent symbols), was provided considering the resulting group delay and its relationship with the minimum redundancy required for destructive IBI-free transmissions. Theoretical results showed the monotonicity of the spectral efficiency with respect to the sampling time, as well as the minimum sampling time to guarantee information-losslessness transmissions as a function of the roll-off factor of the transmitting filter, the frequency-packing factor, and the number of subcarriers. Numerical results corroborated the theoretical predictions and showed that the proposed schemes can outperform zero-forcing precoders in terms of achieving a better balance between spectral and energy efficiencies. Future works include formulating and efficiently solving the problem of optimally setting the group delay of the effective channel model, analyzing the achievable rate of the proposed transceivers through an information-theoretic approach, as well as clarifying the relationship between the number of redundant signals and an achievable symbol error rate performance.

APPENDIX A
PROOF OF PROPOSITION 1

For fixed β, b, r_c, ρ, M, as $\mathrm{SE}_0(\alpha, \beta) \propto \frac{M}{M+R_{\alpha,\beta}} \frac{1}{\alpha}$ and

$$\begin{aligned} \frac{M}{M+R_{\alpha,\beta}} \frac{1}{\alpha} &= \frac{M}{\alpha M + \alpha \left\lfloor \frac{\alpha'}{\alpha} R_{\alpha',\beta} \right\rfloor} \\ &\geq \frac{M}{\left(\frac{\alpha}{\alpha'}\right) M + R_{\alpha',\beta}} \frac{1}{\alpha'} \\ &= \frac{M}{M+R_{\alpha',\beta}} \frac{1}{\alpha'} \left(\frac{1}{1 - \frac{\left[1-\left(\frac{\alpha}{\alpha'}\right)\right] M}{M+R_{\alpha',\beta}}} \right), \end{aligned} \tag{43}$$

then, when $\alpha < \alpha'$, one has $\frac{\left[1-\left(\frac{\alpha}{\alpha'}\right)\right] M}{M+R_{\alpha',\beta}} < 1$, thus implying that $\frac{M}{M+R_{\alpha,\beta}} \frac{1}{\alpha} > \frac{M}{M+R_{\alpha',\beta}} \frac{1}{\alpha'} \Leftrightarrow \mathrm{SE}_0(\alpha, \beta) > \mathrm{SE}_0(\alpha', \beta)$.

APPENDIX B
PROOF OF PROPOSITION 3

From Lemma 1, we note that the necessary and sufficient condition for information losslessness can be rewritten as $\tilde{F}^2(\mathrm{j}\omega) > 0, \forall \omega \in \mathbb{R}$, for $\tilde{F}^2(\mathrm{j}\omega) \triangleq \sum_{i \in \mathbb{Z}} \left| F\left(\mathrm{j}\frac{(\omega+2\pi i)}{T_\mathrm{s}}\right) \right|^2$. As $f(t)$ is a square-root T_β-Nyquist filter with roll-off ρ, then $F\left(\mathrm{j}\frac{(\omega+2\pi i)}{T_\mathrm{s}}\right) = F\left(\frac{\mathrm{j}}{\alpha}\frac{(\omega+2\pi i)}{T_1}\right) = 0$ for $\omega \notin \left(-\frac{\alpha\xi_M(\beta)(1+\rho)\pi}{T_1} - \frac{2\pi i}{T_1}, \frac{\alpha\xi_M(\beta)(1+\rho)\pi}{T_1} - \frac{2\pi i}{T_1}\right)$. In this case,

$\tilde{F}^2(\mathrm{j}\omega) > 0, \forall\omega \in \mathbb{R}$ iff the intersection of the adjacent supports of $F\left(\mathrm{j}\frac{(\omega+2\pi i)}{T_\mathrm{s}}\right)$ and $F\left(\mathrm{j}\frac{(\omega+2\pi(i+1))}{T_\mathrm{s}}\right)$ is nonempty; iff: $-\frac{\alpha\xi_M(\beta)(1+\rho)\pi}{T_1} - \frac{2\pi i}{T_1} \leq \frac{\alpha\xi_M(\beta)(1+\rho)\pi}{T_1} - \frac{2\pi(i+1)}{T_1} \Leftrightarrow \alpha\cdot\xi_M(\beta)\cdot(1+\rho)\geq 1$.

APPENDIX C
PROOF OF PROPOSITION 4

Based on (29) and (28c), the entries of the backward IBI matrices ($\boldsymbol{H}^{(\mathrm{b})}_{\mathrm{IBI}_{k,n}}[b]$) will be zero when $-bP+p_\mathrm{r}-p_\mathrm{c}+q_\delta P+\rho_\delta<0 \Leftrightarrow p_\mathrm{r}-p_\mathrm{c}<(b-q_\delta)P-\rho_\delta$ for all pair $(p_\mathrm{r},p_\mathrm{c})\in\mathscr{P}^2$. As $p_\mathrm{r}-p_\mathrm{c}\in\{-(P-1),\ldots,(P-1)\}$ and $\rho_\delta\in\mathscr{P}$, the former inequality certainly holds when $b>q_\delta+1$, and it may hold when $b=q_\delta+1$ (whenever $\rho_\delta=0$, i.e., whenever δ is a multiple of P). In other words, $\boldsymbol{H}^{(\mathrm{b})}_{\mathrm{IBI}_{k,n}}[b]=\boldsymbol{0}_{P\times P}$ for $b>q_\delta+1$ or $(b,\rho_\delta)=(q_\delta+1,0)$, thus implying that $\mathscr{B}^{(\mathrm{b})}=\{1,\ldots,q_\delta+1\}$ in general. Similarly, noticing that, based on (30), one can write $\nu=(B-3)P+\rho_\nu+1$, with ρ_ν being an integer number in the set $\mathscr{P}$, then it follows from (28b) that the entries of the forward IBI matrices ($\boldsymbol{H}^{(\mathrm{f})}_{\mathrm{IBI}_{k,n}}[b]$) will be zero when $bP+p_\mathrm{r}-p_\mathrm{c}+q_\delta P+\rho_\delta>(B-3)P+\rho_\nu+1 \Leftrightarrow p_\mathrm{c}-p_\mathrm{r}<[b-(B-3-q_\delta)]P-(1+\rho_\nu-\rho_\delta)$ for all pair $(p_\mathrm{r},p_\mathrm{c})\in\mathscr{P}^2$. As $p_\mathrm{c}-p_\mathrm{r}\in\{-(P-1),\ldots,(P-1)\}$ and $1+\rho_\delta-\rho_\nu\in\{-(P-2),\ldots,P\}$, the former inequality certainly holds when $b>B-2-q_\delta$, and it may hold when $b=B-2-q_\delta$ (whenever $\rho_\delta>\rho_\nu$; in this case, δ is not a multiple of P). In other words, $\boldsymbol{H}^{(\mathrm{f})}_{\mathrm{IBI}_{k,n}}[b]=\boldsymbol{0}_{P\times P}$ for $b>B-2-q_\delta$, or $b=B-2-q_\delta$ and $\rho_\delta>\rho_\nu=\nu-(B-3)P-1$, thus implying that $\mathscr{B}^{(\mathrm{f})}=\{1,\ldots,B-2-q_\delta\}$ in general. Note that, from (29), the group delay satisfies $\delta<\nu$, which implies $(B-2-q_\delta)P>P-(1+\rho_\nu-\rho_\delta)\geq 0$, thus yielding $B-2-q_\delta\geq 1$, so that the set $\mathscr{B}^{(\mathrm{f})}$ is well-defined. From (27), the number of data blocks contributing to the ℓ^{th} received block after sampling, synchronization, and buffering is up to $1+\left|\mathscr{B}^{(\mathrm{f})}\right|+\left|\mathscr{B}^{(\mathrm{b})}\right|=B$ whenever δ is such that $\rho_\delta\in\{1,2,\ldots,\rho_\nu\}$, or otherwise (i.e., $\delta=q_\delta P+\rho_\delta$, with $q_\delta\in\mathbb{N}$ and $\rho_\delta\in\mathscr{P}\setminus\{1,2,\ldots,\rho_\nu\}$) up to $B-1$.

APPENDIX D
PROOF OF PROPOSITION 5

Firstly, note that $\boldsymbol{R}\boldsymbol{H}^{(\mathrm{b})}_{\mathrm{IBI}_{k,n}}[b]\boldsymbol{A}$ is an $M\times M$ matrix comprised of the entries $\left[\boldsymbol{H}^{(\mathrm{b})}_{\mathrm{IBI}_{k,n}}[b]\right]_{p_\mathrm{r},p_\mathrm{c}}$, with $p_\mathrm{r}\in\{0,\cdots,M-1\}$ and $p_\mathrm{c}\in\{P-M,\cdots,P-1\}$. From (28c), backward-IBI-free transmissions are possible when $-bP+p_\mathrm{r}-p_\mathrm{c}+\delta<0$ for all $b\in\mathscr{B}^{(\mathrm{b})}$, $p_\mathrm{r}\in\{0,\cdots,M-1\}$, and $p_\mathrm{c}\in\{P-M,\cdots,P-1\}$. The maximum value that the L.H.S. of the former inequality can assume occurs when $(b,p_\mathrm{r},p_\mathrm{c})=(1,M-1,M-P)$. Thus, recalling that $P=M+R$, one must have $-(M+R)+(M-1)-R+\delta<0\Leftrightarrow 2R>\delta-1$, from which (34) follows.

ACKNOWLEDGMENT

For the purpose of open access, the authors have applied a Creative Commons Attribution 4.0 International (CC BY 4.0) license to any Author Accepted Manuscript version arising from this submission.

REFERENCES

[1] F. Rusek and J. B. Anderson, "The two dimensional Mazo limit," in *Proc. IEEE Int. Symp. Inf. Theory (ISIT)*, Sep. 2005, pp. 970–974.
[2] J. B. Anderson, F. Rusek, and V. Öwall, "Faster-than-Nyquist signaling," *Proc. IEEE*, vol. 101, no. 8, pp. 1817–1830, Aug. 2013.
[3] C. Masouros and E. Alsusa, "Dynamic linear precoding for the exploitation of known interference in MIMO broadcast systems," *IEEE Trans. Wireless Commun.*, vol. 8, no. 3, pp. 1396–1404, Mar. 2009.
[4] C. Masouros and E. Alsusa, "Soft linear precoding for the downlink of DS/CDMA communication systems," *IEEE Trans. Veh. Technol.*, vol. 59, no. 1, pp. 203–215, Jan. 2010.
[5] C. Masouros, "Correlation rotation linear precoding for MIMO broadcast communications," *IEEE Trans. Signal Process.*, vol. 59, no. 1, pp. 252–262, Jan. 2011.
[6] M. Alodeh, S. Chatzinotas, and B. Ottersten, "Constructive multiuser interference in symbol level precoding for the MISO downlink channel," *IEEE Trans. Signal Process.*, vol. 63, no. 9, pp. 2239–2252, May 2015.
[7] M. Alodeh, S. Chatzinotas, and B. Ottersten, "System and device for symbol-level multiuser precoding," WO Patent 2017050930, Mar. 2017.
[8] C. Masouros and G. Zheng, "Exploiting known interference as green signal power for downlink beamforming optimization," *IEEE Trans. Signal Process.*, vol. 63, no. 14, pp. 3628–3640, Jul. 2015.
[9] M. Alodeh, S. Chatzinotas, and B. Ottersten, "Energy-efficient symbol-level precoding in multiuser MISO based on relaxed detection region," *IEEE Trans. Wireless Commun.*, vol. 15, no. 5, pp. 3755–3767, May 2016.
[10] M. Alodeh, S. Chatzinotas, and B. Ottersten, "Symbol-level multiuser MISO precoding for multi-level adaptive modulation," *IEEE Trans. Signal Process.*, vol. 16, no. 8, pp. 5511–5524, Aug. 2017.
[11] D. Spano, M. Alodeh, S. Chatzinotas, and B. Ottersten, "Symbol-level precoding for the nonlinear multiuser MISO downlink channel," *IEEE Trans. Signal Process.*, vol. 66, no. 5, pp. 1331–1345, Jan. 2018.
[12] Y. Choi, J. Lee, M. Rim, and C. G. Kang, "Constructive interference optimization for data-aided precoding in multi-user MISO systems," *IEEE Trans. Wireless Commun.*, vol. 18, no. 2, pp. 1128–1141, Feb. 2019.
[13] M. Alodeh *et al.*, "Symbol-level and multicast precoding for multiuser multiantenna downlink: A state-of-the-art, classification, and challenges," *IEEE Commun. Surveys Tuts.*, vol. 20, no. 3, pp. 1733–1757, 3rd Quart., 2018.
[14] A. Li *et al.*, "A tutorial on interference exploitation via symbol-level precoding: Overview, state-of-the-art and future directions," *IEEE Commun. Surveys Tuts.*, vol. 22, no. 2, pp. 796–839, 2020.
[15] J. E. Mazo, "Faster-than-Nyquist signaling," *Bell Syst. Tech. J.*, vol. 54, no. 8, pp. 1451–1462, 1975.
[16] A. D. Liveris and C. N. Georghiades, "Exploiting faster-than-Nyquist signaling," *IEEE Trans. Commun.*, vol. 51, no. 9, pp. 1502–1511, Sep. 2003.
[17] Y. J. D. Kim, J. Bajcsy, and D. Vargas, "Faster-than-Nyquist broadcasting in Gaussian channels: Achievable rate regions and coding," *IEEE Trans. Commun.*, vol. 64, no. 3, pp. 1016–1030, Mar. 2016.
[18] Q. Li, F.-K. Gong, P.-Y. Song, and S.-H. Zhai, "Pre-equalized interference cancellation for faster-than-Nyquist signaling," *IEEE Access*, vol. 7, pp. 77868–77876, 2019.
[19] M. Alodeh, D. Spano, S. Chatzinotas, and B. Ottersten, "Faster-than-Nyquist spatiotemporal symbol-level precoding in the downlink of multiuser MISO channels," in *Proc. IEEE Int. Conf. Acoust., Speech Signal Process. (ICASSP)*, Mar. 2017, pp. 3779–3783.
[20] M. Alodeh, D. Spano, and S. Chatzinotas, "Spatiotemporal precoding for faster-than-Nyquist signal transmissions," CN Patent 110870213, Mar. 2020.
[21] T. Xu, C. Masouros, and I. Darwazeh, "Waveform and space precoding for next generation downlink narrowband IoT," *IEEE Internet Things J.*, vol. 6, no. 3, pp. 5097–5107, Jun. 2019.
[22] M. Jana, L. Lampe, and J. Mitra, "Precoded time-frequency-packed multicarrier faster-than-Nyquist transmission," in *Proc. IEEE Int. Workshop Signal Process. Adv. Wireless Commun. (SPAWC)*, Jul. 2019, pp. 1–5.
[23] W. A. Martins, D. Spano, S. Chatzinotas, and B. Ottersten, "Faster-than-Nyquist signaling via spatiotemporal symbol-level precoding for multiuser MISO redundant transmissions," in *Proc. IEEE Int. Conf. Acoust., Speech Signal Process. (ICASSP)*, May 2020, pp. 5090–5094.
[24] P. S. R. Diniz, W. A. Martins, and M. V. S. Lima, *Block Transceivers: OFDM and Beyond*. Morgan & Claypool. San Rafael, CA, USA: 2012.
[25] T. K. Y. Lo, "Maximum ratio transmission," *IEEE Trans. Commun.*, vol. 47, no. 10, pp. 1458–1461, Oct. 1999.

[26] M. Joham, W. Utschick, and J. A. Nossek, "Linear transmit processing in MIMO communications systems," *IEEE Trans. Signal Process.*, vol. 53, no. 8, pp. 2700–2712, Aug. 2005.
[27] A. Scaglione, G. B. Giannakis, and S. Barbarossa, "Redundant filterbank precoders and equalizers. I. Unification and optimal designs," *IEEE Trans. Signal Process.*, vol. 47, no. 7, pp. 1988–2006, Jul. 1999.
[28] Y.-P. Lin and S.-M. Phoong, "Minimum redundancy for ISI free FIR filterbank transceivers," *IEEE Trans. Signal Process.*, vol. 50, no. 4, pp. 842–853, Apr. 2002.
[29] W. A. Martins and P. S. R. Diniz, "Minimum redundancy multicarrier and single-carrier systems based on Hartley transforms," in *Proc. Eur. Signal Process. Conf. (EUSIPCO)*, Aug. 2009, pp. 661–665.
[30] W. A. Martins and P. S. R. Diniz, "Block-based transceivers with minimum redundancy," *IEEE Trans. Signal Process.*, vol. 58, no. 3, pp. 1321–1333, Mar. 2010.
[31] W. A. Martins and P. S. R. Diniz, "Memoryless block transceivers with minimum redundancy based on Hartley transforms," *Signal Process.*, vol. 91, no. 2, pp. 240–251, 2011. [Online]. Available: http://www.sciencedirect.com/science/article/pii/S0165168410002847
[32] W. A. Martins and P. S. R. Diniz, "LTI transceivers with reduced redundancy," *IEEE Trans. Signal Process.*, vol. 60, no. 2, pp. 766–780, Feb. 2012.
[33] W. A. Martins and P. S. R. Diniz, "DHT-based transceivers with reduced redundancy," *IEEE Trans. Signal Process.*, vol. 60, no. 11, pp. 6080–6085, Nov. 2012.
[34] D. H. Bailey and P. N. Swarztrauber, "The fractional Fourier transform and applications," *SIAM Rev.*, vol. 33, no. 3, pp. 389–404, Sep. 1991.
[35] P. P. Vaidyanathan, S.-M. Phoong, and Y.-P. Lin, *Signal Processing and Optimization for Transceiver Systems*. Cambridge, U.K.: Cambridge Univ. Press, 2010.
[36] M. H. M. Costa, "Writing on dirty paper (corresp.)," *IEEE Trans. Inf. Theory*, vol. IT-29, no. 5, pp. 439–441, May 1983.
[37] M. Grant, S. Boyd, and Y. Ye, "Disciplined convex programming," in *Global Optimization: From Theory to Implementation*, L. Liberti and N. Maculan, Eds. Boston, MA, Springer, 2006, pp. 155–210, ch. 7.
[38] D. Spano, S. Chatzinotas, and B. Ottersten, "Sequential spatia-temporal symbol-level precoding enabling Faster-than-Nyquist signaling for multi-user MISO systems," in *Proc. 26th Eur. Signal Process. Conf. (EUSIPCO)*, Sep. 2018, pp. 827–831.
[39] D. Spano, M. Alodeh, S. Chatzinotas, and B. Ottersten, "Faster-than-Nyquist signaling through spatio-temporal symbol-level precoding for the multiuser MISO downlink channel," *IEEE Trans. Wireless Commun.*, vol. 17, no. 9, pp. 5915–5928, Sep. 2018.
[40] A. Haqiqatnejad, "Enhanced signal space design for multiuser MIMO interference channels," Ph.D. dissertation, Doctoral School in Sci. Eng. (DSSE), Univ. Luxembourg, Interdisciplinary Centre Secur., Rel. Trust (SnT), Esch-sur-Alzette, Luxembourg, 2021. [Online]. Available: https://orbilu.uni.lu/handle/10993/46253
[41] R. A. Polyak, "Projected gradient method for non-negative least square," *Contemp. Math.*, vol. 636, pp. 167–179, Mar. 2015.

Wallace Alves Martins (Senior Member, IEEE) received the degree in electronics engineering, and the M.Sc. and D.Sc. degrees in electrical engineering from the Federal University of Rio de Janeiro (UFRJ), Rio de Janeiro, Brazil, in 2007, 2009, and 2011, respectively. He was a Research Visitor at the University of Notre Dame, USA, in 2008, Université de Lille 1, France, in 2016, and Universidad de Alcalá, Spain, in 2018. He was an Associate Professor at the Department of Electronics and Computer Engineering (DEL/Poli) and the Electrical Engineering Program (PEE/COPPE), UFRJ, from 2013 to 2022. He was an Academic Coordinator and the Deputy Department Chairman (DEL/Poli), UFRJ, from 2016 to 2017. He is currently a Research Scientist working with the Interdisciplinary Centre for Security, Reliability and Trust (SnT), University of Luxembourg. His research interests include digital signal processing and telecommunications, with focus on equalization and beamforming/precoding for terrestrial and non-terrestrial (satellite) wireless communications. He is a member (Associate Editor) of the Editorial Boards of the IEEE SIGNAL PROCESSING LETTERS and the *EURASIP Journal on Advances in Signal Processing*. He was a recipient of the Best Student Paper Award from EURASIP at EUSIPCO-2009, Glasgow, Scotland, the 2011 Best Brazilian D.Sc. Dissertation Award from CAPES, and the Best Paper Award at SBrT-2020, Florianópolis, Brazil.

Symeon Chatzinotas (Senior Member, IEEE) received the M.Eng. degree in telecommunications from the Aristotle University of Thessaloniki, Thessaloniki, Greece, in 2003, and the M.Sc. and Ph.D. degrees in electronic engineering from the University of Surrey, Surrey, U.K., in 2006 and 2009, respectively. He was a Visiting Professor at the University of Parma, Italy, and he was involved in numerous Research and Development projects for the National Center for Scientific Research Demokritos, the Center of Research and Technology Hellas, and the Center of Communication Systems Research, University of Surrey. He is currently a Full Professor, the Chief Scientist I, and the Co-Head of the SIGCOM Research Group with SnT, University of Luxembourg. He has coauthored more than 400 technical papers in refereed international journals, conferences, and scientific books. He was a corecipient of the 2014 IEEE Distinguished Contributions to Satellite Communications Award, the CROWNCOM 2015 Best Paper Award, and the 2018 EURASIC JWCN Best Paper Award. He is currently with the Editorial Board of the IEEE OPEN JOURNAL OF VEHICULAR TECHNOLOGY and the *International Journal of Satellite Communications and Networking*.

Björn Ottersten (Fellow, IEEE) was born in Stockholm, Sweden, in 1961. He received the M.S. degree in electrical engineering and applied physics from Linköping University, Linköping, Sweden, in 1986, and the Ph.D. degree in electrical engineering from Stanford University, Stanford, CA, USA, in 1990.

He had held research positions at the Department of Electrical Engineering, Linköping University, the Information Systems Laboratory, Stanford University, the Katholieke Universiteit Leuven, Leuven, Belgium, and the University of Luxembourg, Luxembourg. From 1996 to 1997, he was the Director of Research at ArrayComm, Inc.—a start-up in San Jose, CA, USA, based on his patented technology. In 1991, he was a Professor of signal processing with the Royal Institute of Technology, Stockholm. From 1992 to 2004, he was the Head of the Department for Signals, Sensors, and Systems, KTH, and from 2004 to 2008, he was the Dean of the School of Electrical Engineering. He is currently the Director of the Interdisciplinary Centre for Security, Reliability and Trust, University of Luxembourg.

Dr. Ottersten has coauthored journal articles that received the IEEE Signal Processing Society Best Paper Award in 1993, 2001, 2006, and 2013, and seven IEEE Conference Papers Best Paper Awards. He was a recipient of the IEEE Signal Processing Society Technical Achievement Award in 2011 and twice a recipient of the European Research Council Advanced Research Grant from 2009 to 2013 and from 2017 to 2022. He was an Associate Editor of the IEEE TRANSACTIONS ON SIGNAL PROCESSING and the Editorial Board of the *IEEE Signal Processing Magazine*. He is currently a member of the Editorial Boards of the *EURASIP Signal Processing Journal*, the *EURASIP Journal of Advances in Signal Processing*, and the Foundations and Trends of Signal Processing. He is a fellow of EURASIP.